NASA

Technical Memorandum 83891

The Tropospheric Gas Composition of Jupiter's North Equatorial Belt (NH_3, PH_3, CH_3D, GeH_4, H_2O) and the Jovian D/H Isotopic Ratio

V. Kunde, R. Hanel, W. Maguire, D. Gautier,
J.P. Baluteau, A. Marten, A. Chedin,
N. Husson, and N. Scott

FEBRUARY 1982

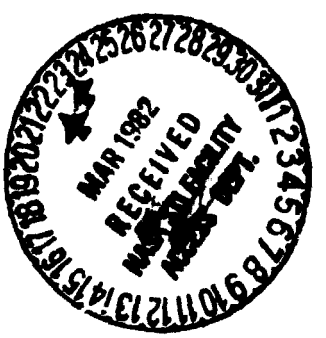

National Aeronautics and
Space Administration

Goddard Space Flight Center
Greenbelt, Maryland 20771

The Tropospheric Gas Composition of Jupiter's North Equatorial Belt (NH_3, PH_3, CH_3D, GeH_4, H_2O) and the Jovian D/H Isotopic Ratio

by

V. Kunde, R. Hanel, W. Maguire
Laboratory for Extraterrestrial Physics
NASA/Goddard Space Flight Center
Greenbelt, MD 20771

and

D. Gautier, J. P. Baluteau, A. Marten
Observatoire de Paris
92190 Meudon, France

and

A. Chedin, N. Husson, N. Scott
Laboratoire de Meteorologie Dynamique du CNRS
Ecole Polytechnique
Palaiseau, France

February 1982

Submitted for publication in
The Astrophysical Journal

ABSTRACT

The gas composition of the troposphere of Jupiter in the clearest regions of the North Equatorial Belt (NEB) was derived from the Voyager 1 IRIS data. The infrared spectrum for this homogenous "cloud-free" region was modeled to infer altitude profiles for NH_3, PH_3, CH_3D, GeH_4 and H_2O. The profiles for NH_3 and PH_3 were found to be depleted in the upper troposphere but otherwise in agreement with their solar values at the 1 bar level. The mole fraction for CH_3D was determined to be $3.5^{+1.0}_{-1.3}\times10^{-7}$. The GeH_4 mole fraction of $7\pm2\times10^{-10}$ at the 2-5 bar level is a factor of 10 lower than the solar value. The H_2O mole fraction is $\sim1\times10^{-6}$ at the 2.5 bar level and is increasing to $\sim3\times10^{-5}$ at 4 bars where it is a factor of 30 lower than solar. Using IRIS inferred values for the mole fractions of CH_3D and CH_4 a value of D/H = $3.6^{+1.0}_{-1.4}\times10^{-5}$ is derived. Assuming this Jovian D/H ratio is representative of the protosolar nebula, and correcting for chemical galactic evolution, yields a value of $5.5\text{-}9.0\times10^{-5}$ for the primordial D/H ratio and an upper limit of $1.8\text{-}2.4\times10^{-31}$ gm/cm^3 for the present day baryon density.

Subject Headings: infrared: spectra-abundances-planets: atmospheres-planets: Jupiter-planets: spectra

I. INTRODUCTION

Knowledge of the atmospheric composition and its vertical and horizontal variation is important for understanding the physical and chemical processes presently active on Jupiter. Information on the relative elemental abundances and their isotopic ratios, which may also be inferred from molecular abundances, help in a better understanding of the formation and evolution of Jupiter and the solar system as a whole. Because of the large mass and low exospheric temperatures Jupiter is believed to still have primordial composition. Comparison of Jovian abundances with corresponding solar values is thus equally important for theories of Jovian, solar and solar system evolution. Analysis of the thermal emission spectrum allows detection and in some cases measurement of vertical distributions of several gases. This paper discusses the chemical composition and physical state of the Jovian atmosphere between 0.2 and 5 bar in the North Equatorial Belt.

In the last decade ground-based and airborne spectral measurements of the emitted infrared radiation have produced extensive information on the gaseous composition of the Jovian atmosphere (Encrenaz and Combes 1981; Larson 1977; Ridgway et al. 1976a). The accuracy of these results, however, has often been limited by the lack of spatial resolution, and the ensuing complications in interpretation due to inhomogeneous cloud fields.

The Voyager IRIS (Infrared Interferometer Spectrometer and Radiometer) measurements cover the spectral range from 180 to 2500 cm^{-1} with 4.3 cm^{-1} resolution and offer several important improvements over previous ground-based and airborne data. First, a large number of spectra were obtained at various locations on the disk of the planet with a spatial resolution as high as 1^{o} in Jovian latitude near closest approach. This high spatial resolution allows the separation of characteristic features; thus it is possible to select spectra from belts where the influence of clouds is negligible and from zones where clouds are apparent. Second, the wide spectral range of the IRIS allows the retrieval of temperature structure and composition information simultaneously and within the same volume element, thus eliminating uncertainties due to temporal and spatial variations. Third, the wide spectral range allows also the simultaneous retrieval of the concentrations of several key atmospheric gases.

This paper is concerned with the gaseous composition of the lower atmosphere in the North Equatorial Belt (NEB). Clouds in the equatorial region have been studied by Marten et al. (1981). Section II describes the selection of the spectra. Section III discusses the radiative transfer techniques used to obtain the thermal profile and the composition. Sections IV, V and VI treat the analysis techniques and the results of the molecular composition study. Section VII discusses the D/H isotopic ratio and finally section VIII presents conclusions.

II. OBSERVATIONS AND SELECTION CRITERIA

Approximately 25000 Jovian spectra were acquired by the IRIS during the Voyager 1 flyby for varying latitudes, longitudes, emission angles and local time (Hanel et al. 1979). Different locations on the planet show significant differences in their spectra. For this study the NEB has been chosen for analysis as it represents the most prominent, well defined cloud-free region at the time of the Voyager 1 flyby (Terrile et al. 1979). Furthermore, many observational sequences were aimed at the NEB, thus providing an ample set of spectra. The signal to noise ratio (S/N) for an individual measurement varies across the spectrum, decreasing from ~200 at 200 cm^{-1} to about 5 at 2000 cm^{-1}. Because of the low S/N at 2000 cm^{-1} it is necessary to average a number of individual spectra. The optimum number is a tradeoff between the desired S/N and the required degree of atmospheric homogeneity in the ensemble. The selection criteria applied in this investigation are:

1) Latitudinal extent - The ground-based maps of the Jovian disk at 2000 cm^{-1} show strong emission covering most of the NEB from approximately 8 to 13°N latitude (Terrile et al. 1979). Therefore the center point of the IRIS field of view (FOV) has been restricted to these latitudes.

2) Spatial resolution - To assure that the projected field of view on Jupiter is less than the latitudinal extent of the NEB, only spectra obtained with a spatial resolution of less than 5° in latitude were accepted. All admitted spectra were recorded within ±1 day of closest approach. The highest spatial resolution in the sample is 0.8° in latitude.

3) Emission angle - This angle has been arbitrarily chosen to be less than 30°, corresponding to an air mass of less than 1.15.

The above criteria define an ensemble of spectra for the NEB under near vertical viewing conditions and with sufficient spatial resolution. However, considerable longitudinal atmospheric inhomogeneity can be noted in this ensemble and it is necessary to define two additional criteria to assure selection of the clearest and most homogeneous cases. The continuum levels of the IRIS spectrum near 226 cm^{-1} and 2000 cm^{-1} are very sensitive indicators of the presence of haze and clouds at the .8 bar and 2-3 bar levels, respectively. The highest brightness temperatures correspond to the clearest conditions. Two other selection criteria are therefore added:

4) 226 cm^{-1} continuum - Only spectra with brightness temperatures higher than 149K at 226 cm^{-1} have been selected, and,

5) 2000 cm^{-1} continuum - Only spectra with an average brightness temperature higher than 250K averaged over 1950-2150 cm^{-1} were accepted.

Out of 25207 only 51 spectra passed all five criteria. The average spectrum and the standard deviation (δT_{BB}) of this ensemble are shown in Figs. 1 and 2. The average air mass factor for this ensemble is 1.04, corresponding to an equivalent emission angle of 15.8°. The S/N of the average spectrum is $\sim$1400 at 200 cm^{-1}, decreasing to $\sim$35 at 2000 cm^{-1}. The standard deviations shown in Figs. 1b and 2b are due mostly to longitudinal inhomogeneities in the troposphere of the NEB, the instrument noise being a factor of $\sim$10 lower. In spite of this, the relatively small amplitude of the standard deviation indicates that the average spectrum represents a fairly homogenous region.

The average spectrum shows the signatures of H_2, CH_4, C_2H_2, NH_3, PH_3, H_2O, GeH_4 and CH_3D. The spectrum divides naturally into two regimes: 180-1500 cm^{-1} (Fig. 1), which corresponds to thermal emission mostly from above the one bar level and 1800-2250 cm^{-1} (Fig. 2), which corresponds to emission mostly from below that level. The altitude from which the maximum contribution to the emission originates (unit optical depth) is illustrated in

Figs. 3 and 4. These 1/e levels have been computed with the help of the model atmosphere described in Section III. It is evident from Figs. 3 and 4 that the IRIS NEB spectrum contains information on the abundances of NH_3, PH_3, CH_3D, H_2O, and GeH_4 between approximately .2 and 5 bar. The information on the relevant altitudes will be discussed for each gas individually after presentation of the appropriate radiative transfer equation and the analysis procedures.

III. RADIATIVE TRANSFER ASPECTS

Retrieval of the thermal structure is the first step in the abundance determination. Vertical temperature profiles have been inferred from the IRIS spectrum by inversion of the radiative transfer equation, using measurements at selected wave numbers within the S(0) and S(1) lines of H_2 (285-610 cm^{-1}), and in the core of the ν_4 band of CH_4 (1250-1350 cm^{-1}). A CH_4 mole fraction of 1.75×10^{-3} was assumed, which is 2.07 times the solar value (Gautier et al. 1982). Preliminary Jovian temperature profiles from Voyager IRIS data have been presented by Hanel, et al. (1979), with inversion techniques and typical weighting functions illustrated by Conrath and Gautier (1979), Gautier et al. (1977), and Conrath and Revah (1972). Figure 5 shows the profile retrieved from the spectrum of Fig. 1. Information on the thermal structure is limited to the pressure range from 0.001 to 0.8 bar. To derive temperatures down to 5 bar, which is necessary for analysis of the 2000 cm^{-1} window measurements, the IRIS profile has been extrapolated to deeper levels with an adiabatic lapse rate calculated for a hydrogen mole fraction of 0.90 (Gautier et al. 1981) and taking into account the variation of specific heat with temperature. The dashed curve in Fig. 5 represents this extrapolation.

After the temperature profile is established, the gas abundances may be determined. A "best fit" approach has been used for the retrieval of vertical distributions, except for NH_3 where the inversion method of Smith (1970) was used. In the "best fit" approach spectra are synthesized using the radiative transfer equation, the derived temperature profile and assumed vertical distributions of the absorbing gases. The gas distributions are then iterated until the synthetic and observed spectra agree within error limits.

The monochromatic radiance for vertical viewing of a planetary atmosphere in local thermodynamic equilibrium is

$$I(\nu) = \int B(\nu,T)\, d\tau(\nu,P) \tag{1}$$

where the integration is from the top of the atmosphere down to a lower boundary; B is the Planck function at temperature T and wave number ν. The monochromatic slant path transmittance through an inhomogeneous medium is

$$\tau(\nu,P) = \exp\left[-(L_g + L_h)\right] \tag{2}$$

The optical depth, L_g, of a mixture of gases is

$$L_g = \int \sum_i C\, k^i(\nu,P,T)\, (q^i/g)\, dP \tag{3}$$

with C a constant, P pressure, g gravity, k^i the molecular absorption coefficient, q_i the mole fraction for the ith gas which is defined by

$$q_i = \frac{P_i}{P_{H_2} + P_{He} + \ldots} \quad , \tag{4}$$

and P_i the partial pressure of the ith gas. The haze optical depth is

$$L_h = \int \sigma\, N(z)\, dz = \sigma\, N(z_o)\, e^{-\left[\frac{(z-z_o)}{H_h}\right]} \tag{5}$$

where σ is the extinction cross section, N(z) the number density at altitude z, z_o the altitude at the base of haze layer, and H_h the haze scale height. Only the absorption cross-section of the haze is included in this formulation, with scattering effects neglected. In the 180-1500 cm^{-1} range, the effect of haze is negligible for the NEB (Marten et al. 1981). Thus, the haze has been included only in the analysis of the 1850-2250 cm^{-1} region. The computed monochromatic radiances are convolved with the IRIS instrument function to obtain synthetic spectra with a resolution compatible with the measured spectra. The radiance and transmittance calculations rely on a multi-layer model of the atmosphere and on a direct spectral integration procedure (Scott and Chedin 1981; Kunde and Maguire 1974; Scott 1973) for absorption by H_2,

CH_4, NH_3, PH_3, CH_3D, H_2O, and GeH_4. The distributions for NH_3 and H_2O were also required not to exceed saturation. The molecular parameters used have been assembled into a line atlas as detailed in Appendix A.

The shapes of absorption lines were described by the Voigt line shape for pressures less than 0.1 bar and by the collisionally-broadened Lorentz shape for pressures greater than 0.1 bar. It is generally agreed that for pressures larger than 0.1 bar the Lorentz profile is appropriate for the cores of the lines, but it is uncertain how far into the wings it is valid. Theoretical and experimental studies indicate an exponential modification to the Lorentz line shape in the far wings of absorption bands for CO_2 and other species (Birnbaum 1979, Winters et al. 1964). Such a sub-Lorentzian behavior dramatically affects calculations of the continuum opacity in atmospheric "windows". The far wing effect on the continuum regions in the IRIS spectrum has been discussed by Kunde (1982). In the absence of information on the real behavior of the far wings of absorption lines considered here, we have simulated the sub-Lorentzian behavior by limiting the calculation of the Lorentz profile to a certain spectral distance from the center of each line. In the 180-1500 cm^{-1} range, we have limited calculations to 1200 half-widths from the line center at each atmospheric level (corresponding to α_o = .075 cm^{-1} at 1 bar and 170K), although tests were made for other values of the cut off. In the 1800-2250 cm^{-1} range, calculations were limited to 250 cm^{-1} from the line center at each atmospheric level. The coefficient of 0.5 used for the temperature dependence of the line half-widths is in accord with kinetic theory.

IV. GAS DISTRIBUTIONS FROM THE 180-1200 cm^{-1} RANGE

The gas distributions for NH_3, CH_3D, and PH_3 between .2 and 1 bar have been inferred from the 180-1300 cm^{-1} portion of the NEB spectrum, using the temperature profile illustrated in Figure 5. The determination of the individual mole fractions from the 850-1300 cm^{-1} interval is difficult due to the overlapping absorption of these gases as illustrated in Fig. 6. The homogeneous path spectrum of each gas is computed for the average temperature (125K), pressure (.4 bar), and optical pathlength (U in cm atm at NTP) down to .8 bar. The absorption by NH_3 is found to dominate from 850 to 1100 cm^{-1}, and

by CH_4 from 1180 to 1450 cm^{-1}. The effect of CH_3D is noticeable between 1120 and 1220 cm^{-1} and of PH_3 between 1100 and 1200 cm^{-1}. The strategy adopted to infer the gas distributions from the measured spectrum, while also accounting for these overlapping effects, was to first determine the NH_3 distribution, then the CH_3D distribution using the inferred NH_3, and finally the PH_3 distribution using the inferred NH_3 and CH_3D data. This process was then iterated until all gas distributions converged.

Ammonia (NH_3)

Gaseous NH_3 is the dominant molecular opacity over a large fraction of the thermal spectrum (see Figs. 3 and 4). Examination of the 1/e curve indicates that NH_3 information may be inferred from the IRIS spectrum over .2-.8 bar from 850-1100 cm^{-1} and over .6-1 bar from 180-300 cm^{-1}. Computed spectra assuming the solar value of 1.78×10^{-4} (Lambert 1978) for the well-mixed region and following the NH_3 saturation in the upper troposphere (Fig. 16) are compared to the observed spectra in Figs. 7a and 8. The comparison for both spectral ranges indicates depletion of NH_3 between .2 and .8 bar.

At the .6-.8 bar level, common to both spectral ranges, one unique NH_3 distribution should satisfy portions of both spectral ranges which correspond to the common weighting functions. However, an initial attempt to retrieve the NH_3 distribution from both 180-300 and 850-1100 cm^{-1} was unsuccessful as both could not be simultaneously fit with the same distribution. The fit from 850-1100 cm^{-1} was excellent, while the fit from 180-300 cm^{-1} was only fair since the calculated spectra exhibit a slope different from that of the observed. The inferred profiles left residual temperature differences of $\sim$1-2K for 180-300 cm^{-1}, which is large compared to instrumental noise (0.03K), whereas from 850-1100 cm^{-1} the residual errors are comparable to the noise level ($\sim$0.7K). The low wave number spectrum shows a systematic trend with maximum disagreement at the lowest wave numbers. Possible sources for this trend include errors in the calibration, the NH_3-H_2, H_2-H_2, and H_2-He absorption coefficients, and the thermal structure. These error sources will be discussed in the next section. Because of this difficulty at low wave numbers, the NH_3 distribution was inferred from 850-1100 cm^{-1} for the .2-.8

bar region; only the continuum in the 180-300 cm^{-1} range was used to derive the well-mixed NH_3 abundance for pressures >.8 atm.

The NH_3 distribution was inferred using the retrieval algorithm of Smith (1970), iterating until the rms radiance residuals were less than 1%. The retrieved profile (Fig. 16) is close to saturation at the .2-.4 mb level, becoming increasingly sub-saturation and reaching a depletion factor of ~3 at .7 bar. This profile then converges with the assumed solar value of $^{q}NH_3 = 1.78 \times 10^{-4}$ (Lambert, 1978) at ~.8 bar. No stratospheric emission from NH_3 is evident in the centers of the two strong Q branches at 930 and 967 cm^{-1}. The synthetic spectrum corresponding to the inferred profile is also shown in Figs. 7a and 8.

An estimate of the error in the inferred NH_3 profile has been made for three pressure levels. The random error in the volume mixing ratio, Δq_r, was determined by perturbing the mixing ratio at a given pressure level until the error in the brightness temperature matched the magnitude of the instrument noise, ΔT_I. The error estimates were evaluated (see Table 1) for three wave numbers which were most sensitive to the given pressure levels. The pressure region over which the perturbation was applied is also given in Table 1. For example, at the .6 atm level, the maximum perturbation was applied at this level, with the perturbation then decreasing linearly in altitude back to the unperturbed values at .4 and .8 atm. Thus each perturbation is localized to an altitude range corresponding to approximately .2 to .3 atm. The larger random error for the .3 atm level is caused by the larger ΔT associated with the colder temperatures and smaller temperature gradient at that level. Systematic errors can also be caused by uncertainties in calibration (Δq_1), temperature structure (Δq_2), and molecular parameters (Δq_3). A systematic relative error of 0.1K in the calibration results in $\Delta q_1/q = 1\%$. An uncertainty in the retrieved profile of $\Delta T = \pm .5K$ yields $\Delta q_2/q = 10\%$. The error in the molecular parameters is estimated to be 5% yielding $\Delta q_3/q = 5\%$. These systematic errors, as well as the total error in the inferred NH_3 distribution, are shown in Table 1. The total error is also illustrated in Fig. 16.

The NH_3 mole fraction in the presumably well-mixed portion of the atmosphere (P > .8 bar) was determined from the three continuum intervals 205-210, 220-230, and 245-250 cm^{-1}. Synthetic comparisons for the 180-300 cm^{-1} range are shown in Fig. 7b for two values of the well-mixed NH_3 mole fraction, .5 solar and 1.5 solar. The synthetic spectra for all three cases show a slope different from that of the observed, with the cross-over occurring at $\sim$230 cm^{-1}. As the instrument noise level is only $\sim$.03K at these wave numbers, a large systematic error is indicated. Possible error sources include errors in the instrument calibration, the retrieved thermal structure, and the NH_3-H_2, H_2-H_2 and H_2-He absorption coefficients. The instrument calibration is not as well known below 200 cm^{-1} as above that wave number because of the steep slope at the edge of the instrument response function. Some uncertainty could also come from the retrieved temperature profile since the residuals calculated in the inversion procedure were significantly above the instrument noise level. But probably most important, the NH_3 continuum in the 180-300 cm^{-1} region is mainly formed by the far wings of the strong rotational lines ($\Delta\nu \gtrsim$ 50-100 cm^{-1}) for which the pressure induced H_2-NH_3 line shape is unknown. With this uncertainty it is not possible to infer precisely the NH_3 mole fraction from the low wave number spectrum. Visual comparison of the observed and synthetic spectra in the three continuum regions suggests a value for the well-mixed region which is consistent with the solar value ($^qNH_3$ = 1.78±.89x10^{-4}) and an uncertainty of a factor 2. Thus the error of the NH_3 mole fraction in the well-mixed region is entirely due to systematic errors in the 180-300 cm^{-1} range.

In principle, information on the NH_3 abundance in the well-mixed region is also available from $\sim$1150 cm^{-1} where the emission originates at about 0.8-0.9 bar. In this spectral range the absorption is mainly determined by the wings of strong absorption lines of NH_3 and CH_4. As mentioned previously, the value of the absorption in atmospheric windows strongly depends on the assumed line shape for the far wings of collisional broadened lines. An example of the resulting uncertainty is given in Fig. 9 where spectra have been computed for all gases for Lorentz cut-offs of 100 and 200 cm^{-1}, which corresponds to $\sim$1000 and 2000 half widths at the 1 bar level, respectively. The resultant error in the continuum at 1148 cm^{-1} can be as high as 8K. The large uncertainty in the applicable line shape precludes at the present time

derivation of the well-mixed NH_3 mole fraction from this part of the spectrum also. Inference of the NH_3 abundance in the well-mixed region is thus limited by uncertainties in the far wing line shape for CH_4-H_2 and NH_3-H_2 collisions.

Deuterated Methane (CH_3D)

The ν_6 band of CH_3D has absorption features between ~1120 and 1220 cm^{-1} (Fig. 6c). Synthetic spectra of Jupiter have been computed for uniformly mixed values of $^qCH_3D$ = 2, 4, and 8×10^{-7} as shown in Fig. 10, all other absorber distributions being unchanged. The calculated spectrum is sensitive to the CH_3D abundance over the 1120-1220 cm^{-1} range but a detailed comparison with the measured spectrum indicates that all spectral features can be accounted for by CH_4, NH_3, and PH_3. No unique CH_3D line, not even the Q branch at 1156 cm^{-1}, is evident at the 4.3 cm^{-1} resolution. Thus the accurate determination of $^qCH_3D$ in this spectral interval depends entirely on the CH_3D band contour. The continuum level in this spectral interval is mainly established by the far wings of the NH_3 and CH_4 lines, and thus the inferred value for $^qCH_3D$ is again sensitive to assumptions concerning the far-wing line shape, as illustrated by Fig. 9. To test this sensitivity further, we have calculated synthetic spectra for various values of the Lorentz cut-off up to 2000 half-widths for all absorbers, keeping all abundances unchanged. It was observed that the calculated spectrum was constant when the Lorentz cut-off reached values higher than about 1800 half-widths. Varying then the CH_3D abundance, the best fit with the observed spectrum leads to a mixing ratio $^qCH_3D = 2.7 \times 10^{-7}$, which is thus a lower limit. Taking into considerations the instrument noise (0.7K), the error is $\pm 0.5 \times 10^{-7}$. Note that this lower limit is conservative since it implies a very unlikely high value of the far-wing CH_4 contribution (Gautier et al. 1982). More definitive determination of CH_3D from the 1156 cm^{-1} band will require data with higher spectral resolution than 4.3 cm^{-1} and more accurate knowledge of the NH_3-H_2 and CH_4-H_2 continuum absorption. Better laboratory measurements of line shape parameters are badly needed.

Phosphine (PH_3)

Information on the PH_3 concentration in the upper troposphere may be derived from the 1100-1200 cm^{-1} interval where the ν_4 band of PH_3 has a strong influence (Fig. 6d). Synthetic spectra for two PH_3 distributions (see Fig. 17) are compared to the IRIS observations in Fig. 11. Distribution 1 represents the effect of PH_3 photochemistry only, while the inferred distribution is similar to distribution 2 which includes PH_3-NH_3 coupling (Strobel 1977). Both distributions are normalized in the deep atmosphere to the average value inferred from the 2100-2250 cm^{-1} region ($6x10^{-7}$). The 1100-1200 cm^{-1} range is sensitive to the PH_3 distribution between about .4 and .8 bar. The uppermost curve of Fig. 11 has been computed with only H_2, He, and the inferred PH_3 distribution to aid in the identification of the PH_3 lines used in the analysis. The Q-branch at 1119 cm^{-1} is heavily blended by the NH_3 multiplet, however, it is still valuable as a diagnostic line for determining the PH_3 abundance. Fairly isolated PH_3 P-branch multiplets are seen to occur at 1131, 1152 and 1163 cm^{-1} (lines (2), (3), and (4)).

Comparison of the synthetic and observed spectra show that distribution 1 overestimates the PH_3 absorption at all wave numbers, especially near the Q branch at 1119 cm^{-1}. The inferred distribution, with considerably less PH_3 in the upper troposphere, gives fair agreement for most of the PH_3 features. The remaining discrepancy in the continuum is thought to be due to the errors in the assumed far wing contribution of CH_4 and NH_3 and the CH_3D abundance as discussed before. The error bars shown in Fig. 17 reflect the uncertainty due to instrument noise.

V. GAS DISTRIBUTIONS FROM THE 1800 - 2250 cm^{-1} RANGE

The vertical distributions for PH_3, CH_3D, H_2O and GeH_4 between 1 and 5 bar have been inferred from the 1800-2250 cm^{-1} portion of the NEB spectrum (Fig. 2). As between 850 and 1300 cm^{-1}, the determination of individual mixing ratios is difficult due to overlapping absorption of these gases. This blending is illustrated by the homogeneous path spectra of Fig. 12; the spectrum for each gas is computed for the average temperature (200K), average

pressure (1.25 bar), and optical pathlength (U in cm atm at NTP) down to the 2.5 bar level. Absorption by NH_3 dominates from 1800-1900 cm^{-1}, by H_2O from 1900-2100 cm^{-1}, and by PH_3 from 2100-2250 cm^{-1}. CH_3D influences the 2100-2200 cm^{-1} interval. The previously inferred NH_3 distribution (Fig. 16) was adopted for the analysis in the 1800-2250 cm^{-1} range. The NH_3 concentration in the deep atmosphere cannot be inferred from the 1800-1900 cm^{-1} spectrum because of large uncertainties in the NH_3 band strength and far wing contribution of the ν_4 band at 1627 cm^{-1}; furthermore, the strength for the $2\nu_2^s$ NH_3 band at 1882 cm^{-1} is not available at all. A lower limit of S_b = 0.02 cm^{-2} atm^{-1} has been determined for the $2\nu_2^s$ band from the IRIS spectrum, using the previously inferred NH_3 distribution. Future improvements of the NH_3 absorption parameters for ν_4 and $2\nu_2^s$ will allow the NH_3 distribution in the lower atmosphere to be determined from the 1800-1900 cm^{-1} spectrum. The strategy adopted in this analysis was to first determine the distribution of PH_3, then CH_3D, then GeH_4, and finally H_2O.

The computed spectra (1850-2250 cm^{-1}) shown in Figs. 13, 14 and 15 include the effect of a grey absorbing haze. Spectra computed including only molecular absorption show maximum brightness temperatures of ~270K, about 10K higher than the observed temperatures. At the present time, insufficient knowledge of the cloud and haze structure and their optical properties prevents construction of more accurate models of the opacity; therefore, we have modeled the cloud and haze continuum in the simplest way, which is a uniformly mixed grey haze. The haze optical depth (Equ. 5) was computed for H_h = 35 km, with the quantity $\sigma N(z_o)$ determined by normalizing the computed and observed spectra at 2085 cm^{-1}, the region of greatest molecular transparency. The base of the haze layer was taken at 5 bar (z_o = 0 km). The optical depth of the haze equals 0.54 at 5 bar (279K). The effect of the haze on the atmospheric transmittances and brightness temperatures may be seen in Figs. 4 and 15b, respectively. This ad hoc haze model fits the observed spectrum satisfactorily to first order and, therefore, gives some confidence that it is adequate for inferring molecular gas abundances. The haze model is obviously not unique and other types of haze or cloud models could be developed to account for the residual continuum. The uncertainties in the derived gas distributions from the haze model uncertainties are not quantitatively assessed in this paper, but a rough estimate of the error is included in the total error estimates.

Phosphine (PH_3)

Absorption by PH_3 affects the spectrum from 2050-2225 cm^{-1}, as illustrated in Fig. 13. The spectrum in Fig. 13a has been computed including only continuum absorption (H_2, He, CH_4, haze) and the PH_3 absorption, to aid in the identification of PH_3 lines in the observed spectrum. Fig. 13b shows the comparisons of the observed spectrum to synthetic spectra with PH_3 mole fractions of $4x10^{-7}$ and $8x10^{-7}$. The synthetic spectra in Fig. 13b include the effects of all other absorbing gases, besides PH_3, at their inferred concentrations and the grey haze. The absorption features in the observed spectrum which are strongly influenced by individual PH_3 multiplets are indicated by the vertical dashed lines, numbered (1) through (6). Only line (5) is isolated and unblended, this line is displaced in the synthetic spectrum and should be shifted to higher wave numbers by the increment shown by the short horizontal arrow in Fig. 13a and 13b. This error results from inadequate theoretical line positions for the high J lines of the ν_1 and ν_3 fundamentals. The shifted position agrees with laboratory data. Multiplet (1) is blended with a weak NH_3 line, multiplet (2) with a weak H_2O line, and multiplets (3), (4), and (6) are blended with CH_3D lines. The PH_3 mole fraction was determined from spectral comparisons in two regions: 1) 2150-2170 cm^{-1} - The line to continuum ratio for multiplets (3) and (4) indicates a PH_3 mole fraction from $4-8x10^{-7}$, and 2) 2170-2225 cm^{-1} - The roll-off of the continuum from 2170 cm^{-1} to 2225 cm^{-1}, along the P-branch contour of the ν_1 and ν_3 fundamental bands, also indicates $^{q}PH_3 = 4-8x10^{-7}$. As the same $^{q}PH_3$ value satisfies both diagnostic spectral regions, we adopt $^{q}PH_3 = 6\pm2x10^{-7}$ as the mean value for the 1-4 bar region.

Deuterated Methane (CH_3D)

Absorption lines of the ν_2 band of CH_3D dominate most of the observed spectrum from 2100 to 2200 cm^{-1}. The synthetic spectra of Fig. 14b have been computed for CH_3D mole fractions of $1x10^{-7}$ and $5x10^{-7}$, including the grey haze and the other absorbing gases with their inferred concentrations. The CH_3D mole fraction has been determined from comparison of the observed and synthetic spectra in two regions: 1) 2120-2145 cm^{-1} - Four unblended multiplets of the ν_2 P-branch (P10-P7) lie in this region. Comparison of the

line to continuum ratio gives best agreement with $^{q}CH_3D = 4\text{-}5\times10^{-7}$ (multiplet 1 (P10) does not even appear above the continuum for $^{q}CH_3D = 1\times10^{-7}$); 2) 2200 cm^{-1} - The Q-branch of the ν_2 band at 2200 cm^{-1} is fit best for $^{q}CH_3D = 1\times10^{-7}$. The instrumental noise ($\Delta T = \pm 9K$) allow $^{q}CH_3D$ to range from 0.5 to 4×10^{-7} for the Q-branch region.

The P-branch lines require a higher value of $^{q}CH_3D$ ($4\text{-}5\times10^{-7}$) and the Q-branch a lower value ($.5\text{-}4\times10^{-7}$). This difference probably reflects mostly the uncertainties with establishing the continuum. We adopt $^{q}CH_3D = 3.5^{+1.0}_{-2.5}\times10^{-7}$, to include the range of possible values for both P and Q-branch lines.

Germane (GeH_4)

The strong Q-branch of the ν_3 band of GeH_4 absorbs significantly near 2111 cm^{-1} (Fig. 15). This feature is fairly well isolated from surrounding weak H_2O, CH_3D, and individual PH_3 lines, but it is overlapped by the continuum formed by many weak PH_3 lines, (Fig. 12). The weak P and R lines of GeH_4 are all masked by stronger PH_3 and CH_3D lines and are not apparent in the spectrum. The appearance of the Q-branch but not of any P or R lines in the IRIS spectrum agrees with the higher spectral resolution measurements by Fink, et al. (1978). Comparisons of synthetic with the observed IRIS spectra for the Q-branch yield $^{q}GeH_4 = 7\pm2\times10^{-10}$.

Water Vapor (H_2O)

The high J lines of the ν_2 band of H_2O influence the 1900-2100 cm^{-1} interval (Figs. 12 and 15). All 14 H_2O features identified by Larson, et al. (1975) in the initial detection of H_2O in the Jovian atmosphere are evident in the IRIS spectrum. Six of the fairly isolated H_2O lines are indicated in Fig. 15a. Comparisons to synthetic spectra indicate $^{q}H_2O \simeq 1\times10^{-5}$ at 2.5 bar increasing to $\simeq 3\times10^{-5}$ at 4 bar. These values should be good to approximately a factor of two. The synthetic spectrum corresponding to this distribution is shown in Fig. 15a.

VI. GAS COMPOSITION - DISCUSSION

Ammonia (NH_3)

Ammonia plays an important role in the understanding of the Jovian atmosphere: it is the only observed constituent containing N, thus permitting analysis of the elemental abundances of nitrogen; it must play a role in chemical processes with the detailed reactions still unknown; it is the dominant constituent of the upper clouds; and it is important to meteorology and dynamics because of release and consumption of latent heat in phase changes.

The NH_3 distribution inferred in this investigation is shown in Fig. 16. The vertical distribution of NH_3 in the Jovian atmosphere has been the subject of numerous investigations using ground based data (Baluteau et al. 1980; Encrenaz et al. 1980; Marten et al. 1980; Gautier et al. 1979; Goorvitch et al. 1979; Tokunaga et al. 1979; Baluteau et al. 1978; Erickson et al. 1978; Ridgway et al. 1976b; Lacy et al. 1975); however, these measurements have all been at low spatial resolution, usually for averages over the entire disk, and are therefore not directly comparable to the IRIS NH_3 distribution which is derived for the NEB. Only the recent observations of Tokunaga et al. (1981) resolved the NEB; therefore their derived NH_3 profile is shown in Fig. 16. Fair agreement exists for the .5~.7 bar range with serious differences apparent for lower pressures. The reasons for this discrepancy are not known. The difference does not appear to be in either set of observations as the Q-branch (930 and 970 cm^{-1}) temperatures in both measurements are approximately the same (120K). Differences must therefore be a consequence of different assumptions in the models. A spatially resolved (3 arc sec) vertical distribution of NH_3 in the upper atmosphere has been obtained from IUE observations (Combes et al. 1980) for the Equatorial Zone of Jupiter. The lower portion of this distribution is also shown in Fig. 16. Taking into consideration both errors in the IUE measurement and the possible zone-belt difference in upper atmosphere NH_3, the agreement with the IRIS results is acceptable.

The tropospheric distribution of gaseous NH_3 is controlled by several physical mechanisms; dynamics, phase change and photochemistry. Present atmospheric models do not incorporate all three physical mechanisms simultaneously and thus are unable to predict realistic NH_3 distributions for comparison to data. Additionally, models have only been derived for disk averaged conditions. Two globally averaged representative models from Atreya et al. (1977) are included in Fig. 16 for different assumptions for the eddy diffusion coefficient (K), K = constant and $K \propto 1/m^{1/2}$, where m is the total atmospheric number density. The assumed mixing ratios have been normalized in the deep atmosphere to Lamberts solar value. This comparison should only be made qualitatively as the model conditions, such as solar flux at encounter and spatial resolution, are not appropriate for the Voyager conditions. However it is apparent that comparison of measurements with more comprehensive atmospheric models may yield physical parameters, such as the eddy diffusion coefficient.

It must be emphasized that this depleted NH_3 distribution refers only to the belt region on Jupiter where downward motion is expected to take place. The NH_3 distribution appears to be variable over the planet, with saturation occuring in the upwelling cloudy zones (Marten et al. 1981).

Phosphine (PH_3)

Phosphine is an important trace gas because of its role in both dynamics and chemistry, and its possible association with coloration. Furthermore, PH_3 is an important indicator of nonequilibrium chemical activity in the lower atmosphere, being one of the gases that should not exist in the observable atmosphere on the basis of thermochemical equilibrium models.

The PH_3 distribution inferred in this investigation is shown in Fig. 17. PH_3 was first detected in the 1000 cm^{-1} range by Ridgway et al. (1976b) and in the 2100 cm^{-1} range by Larson et al. (1977) with mole fractions consistent with the solar value of P/H. Beer and Taylor (1979) found PH_3 to be five to eight times lower than Larson et al. (1977). The first evidence of PH_3 depletion in the upper troposphere came from Encrenaz et al. (1978), Tokunaga

et al. (1979), and Encrenaz et al. (1980), who found mole fractions of $\sim 1\text{-}2\times10^{-7}$ in the .2 to .6 bar range. Our results are in agreement with the PH_3 depletion in the upper troposphere and with the Larson et al. (1977) value in the deep atmosphere.

The PH_3 photochemistry was first discussed by Prinn and Lewis (1975), who assumed strong vertical mixing to explain the presence of PH_3 at the .4-4 bar level. Strobel (1977) has pointed out that the NH_3 and PH_3 photochemistry are coupled since both constituents are photolyzed by the same UV radiation at a given pressure level. His calculations indicate that the presence of NH_3 increases the photochemical removal of PH_3 through reactions of NH_3 photolysis products H and NH_2 with PH_3. The photochemical model predictions of Strobel (1977) are included in Fig. 17, where distribution 1 is for phosphine photochemistry only and distribution 2 is for the coupled photochemistry of PH_3 and NH_3. The inferred PH_3 distribution compares favorably with distribution 2. The accuracy of the photochemical model is limited by insufficient knowledge of the key reactions and the reaction rates. Furthermore models apply to mean global conditions rather than to a belt, and the eddy diffusion coefficient is not known. It is assumed to be constant, $K = 2\times10^4$ cm^2/sec, for distribution 1 and 2 (Fig. 17). More definitive conclusions from comparison of theoretical and observed PH_3 distributions require improved models.

Deuterated Methane (CH_3D)

Deuterated methane is important as a tracer for the evolution of Jupiter, the solar system, and the galaxy as well as for cosmology. Fig. 18 shows the CH_3D mole fraction inferred by this investigation. The lower limit of $^qCH_3D = 2.7\pm0.5\times10^{-7}$ was derived from 1120-1220 cm^{-1}, and the value $^qCH_3D = 1\text{-}4.5\times10^{-7}$ from 2100-2200 cm^{-1}. We have adopted a central value of 3.5×10^{-7} along with the upper limit of 4.5×10^{-7} from 2100-2200 cm^{-1}, and the lower limit of 2.2×10^{-7} from 1120-1220 cm^{-1}. The final adopted value for this investigation is $^qCH_3D = 3.5^{+1.0}_{-1.3}\times10^{-7}$. Drossart et al. (1982) have derived a comparable value ($1.8^{+1.4}_{-0.9}\times10^{-5}$) from an IRIS average spectrum from 2100-2200 cm^{-1}, the average consisting of several thousand individual spectra distributed over the Jovian disk.

The first detection of deuterium in the Jovian atmosphere was the measurement of the ν_2 band of CH_3D in the 2100-2200 cm^{-1} interval (Beer and Taylor 1973). They inferred a value of $^qCH_3D = 4.8^{+2.7}_{-1.9}\times10^{-7}$ from a total CH_3D column abundance of 1.3±0.3 cm atm. For internal consistency we have revised this mole fraction by scaling their total CH_3D column abundance to our model atmosphere. The air mass correction of 2 originally included by Beer and Taylor (1973) was not used in our re-determination, in accordance with the revised limb correction given by Beer and Taylor (1978). The revised total CH_3D column abundance is 2.6±0.3 cm atm and the revised value for q is $^qCH_3D = 1.9^{+1.1}_{-.7}\times10^{-7}$. A second set of improved measurements of the ν_2 CH_3D band by Beer and Taylor (1978) yields $^qCH_3D = 2.9^{+1.7}_{-1.2}\times10^{-7}$ derived from a column abundance of 4.0±1.0 cm atm, after normalization to our model atmosphere. Our determination of CH_3D is consistent with the Beer and Taylor values at 3 bar. Encrenaz et al. (1980) have used ground-based observations of the ν_6 band at 1156 cm^{-1} to set an upper limit for $^qCH_3D$ less than 1.8×10^{-7} at 0.4 bar. This value is somewhat lower than the IRIS lower limit of $2.7\pm0.5\times10^{-7}$. One plausible explanation is that the discrepancy arises from the low spatial resolution of the Encrenaz et al. observations and the subsequent spectrum modelling which includes the continuum opacity of an ice cloud model. It is quite possible that the cloud opacity has lowered the line to continuum ratio, thus leading to a lower CH_3D abundance.

Germane (GeH_4)

The calculations of Barshay and Lewis (1978) indicate GeH_4 should not be detectable at the 2-5 bar level under chemical equilibrium conditions. Therefore germane is important as a tracer of vertical motions and non-equilibrium chemistry in the deep atmosphere.

The value of $^qGeH_4$ inferred in this investigation is $7\pm2\times10^{-10}$, which is similar to the value derived from ground-based observations of 5×10^{-10} (Fink et al. 1978). This value is a factor of ~10 lower than the solar value (Cameron 1973). The observed abundance of GeH_4 is consistent with chemical models only if vertical mixing rapidly convects GeH_4 from the ~1000K up to the ~250-300K level. The physical significance of detectable amounts of GeH_4 at 2-5 bar have been discussed by Fink et al. (1978) and Barshay and Lewis (1978).

Water Vapor (H_2O)

Water vapor is a trace gas in the lower Jovian atmosphere and is important for elemental abundances, as it is the dominant oxygen-bearing molecule so far identified, and for meteorology and dynamics, as it liberates and consumes latent heat while changing phase.

This investigation inferred a H_2O concentration of $\sim 1 \times 10^{-6}$ at the 2.5 bar level and gradually increasing to $\sim 3 \times 10^{-5}$ at 4 bar. The initial detection of H_2O from aircraft disk observations was by Larson et al. (1975) who derived a value of $\sim 1 \times 10^{-6}$ from comparison with laboratory spectra. Somewhat higher values have been derived from these observations by Bjoraker et al. (1981) using radiative transfer techniques. The general decrease in the H_2O mole fraction with increasing altitude is consistent with a belt being a downwelling region depleted in its condensible gases. Our mole fraction at the 4 bar level is approximately a factor of 30 lower than the solar value (Cameron 1973). It is conceivable that the water vapor abundance may reach solar proportions at deeper levels (5-10 bar) below the downwelling convective cell or in the zones which cannot be probed because of opaque clouds. If our mole fraction is representative of the bulk atmosphere, and if the atmosphere is representative of the bulk composition of the planet, Jupiter shows a significant depletion in oxygen. An alternate explanation postulates excess of water in zones; the total H_2O content of the atmosphere as a whole may, therefore, still be solar-like (Larson et al. 1975).

VII. D/H ISOTOPIC RATIO

The D/H ratio is important as it yields information on chemical processes in the Jovian atmosphere. Additionally, if the deuterium in the primordial solar nebula in the vicinity of the outer planets did not undergo transformation to helium 3, then the Jovian value should be representative of the solar system at its formation. Due to difficulties in deriving an accurate D/H ratio for the protosolar nebulae from solar composition and wind measurements, the Jovian D/H ratio probably yields the best estimate of D/H in the protosolar nebulae. According to atrophysical theory (Epstein et al. 1976) deuterium originated in the Big Bang, with only modest destruction during subsequent galactic evolution. Observations of the D/H ratio in the

planets, meteorites, and interstellar medium, as well as the cosmological significance have been discussed by Schramm and Wagoner (1974) and Geiss and Reeves (1981). The current state of deuterium abundances is summarized in Table 2 and Fig. 19 for the solar system and the interstellar medium. The shaded area is defined by the 1σ error bars from this investigation.

The D/H ratio has been found to vary significantly between the highly fractionated objects of the inner solar system (Earth, carbonaceous chondrites) and the unfractionated objects of the outer solar system (Jupiter, Saturn, Uranus). Comparisons have indicated an enhancement in D/H of 4–10 for the Earth (Craig 1961; see summary in Geiss and Reeves 1981) and 7–40 for carbonaceous chondrites (Boato 1954; Robert et al. 1977; Robert et al. 1978; Robert et al. 1979; Kolodny et al. 1980) over the values for the outer solar system and for the protosolar nebula. These terrestrial and meteoritic enhancements are generally considered to be caused by fractionation at low temperatures (Geiss and Reeves 1972; Black 1973; Geiss and Reeves 1981). We are concerned with the D/H ratio of the protosolar nebula and the fractionated inner solar system objects will not be discussed.

The D/H ratio by number may be derived from the CH_3D abundance

$$D/H = \frac{q_{CH_3D}}{4\, q_{CH_4}} \; 1/f \qquad (6)$$

where the factor of 4 accounts for the replacement of any one of the four H atoms in CH_4 by one D atom in CH_3D. The deuterium chemical fractionation factor, f,

$$f = [D/H]_{methane}/[D/H]_{hydrogen} \qquad (7)$$

is determined by chemical and convective processes in the deep atmosphere of Jupiter. The derivation of the appropriate value of f has been discussed by Beer and Taylor (1973, 1978), and their value of 1.37 has been adopted. Note, however, that Black (1973) has pointed out that the presence of dust in the Jovian atmosphere could increase considerably the value of f. Prior to the Voyager IRIS determination (Gautier et al. 1982), a large uncertainty existed in the CH_4 mole fraction. Several recent investigations had indicated the

carbon abundance to be enhanced by a factor 2-5 over the solar value (for a review, see Gautier et al. 1982; Wallace and Hunten 1978). Other investigations favor the solar value (Combes and Encrenaz 1979), but these last authors have recently revised their analysis for a greater than solar value (Encrenaz and Combes 1982). In the present investigation we have adopted the CH_4 value of Gautier et al. (1982), derived from the IRIS experiment, which is 2.07 times solar ($^qCH_4 = 1.75 \pm .2 \times 10^{-3}$). To make the comparisons internally consistent, we have normalized all the Jovian D/H ratios inferred from CH_3D measurements to this same value of $^qCH_4$. The D/H ratio for this investigation is $3.6^{+1.0}_{-1.4} \times 10^{-5}$. In general fair agreement exists among the four determinations of D/H from atmospheric CH_3D.

The deuterium abundance of the Jovian atmosphere has also been derived from HD lines. Trauger et al. (1973) measured the $P_4(1)$ line of HD, and by comparison with the $S_4(1)$ line of H_2 inferred a D/H value of $2.1 \pm 0.4 \times 10^{-5}$. Based on new laboratory parameters for the $P_4(1)$ HD line, McKellar et al. (1976) have revised the D/H value to $5.6 \pm 1.4 \times 10^{-5}$. New results by Trauger et al. (1977), based on more recent measurements of the $P_4(1)$ HD line, yield $D/H = 5.1 \pm 0.7 \times 10^{-5}$. The Trauger et al. (1977) HD data have also been analyzed by Combes and Encrenaz (1979) by comparison of the HD line strength to that of a weak CH_4 band. They obtain $D/H = 1.3 \pm 1.0 \times 10^{-5}$ for a solar C/H ratio. Re-normalizing to the 2.07 solar C/H value yields $D/H = (1.0\text{-}2.6) \times 10^{-5}$. The comparison of the D/H ratios inferred from the CH_3D measurements and the HD analysis of Trauger et al. (1973; 1977) indicates a systematic difference. The reanalysis of the HD lines by Combes and Encrenaz (1979) eliminates this difference; all methods, including those using meteoritic and solar wind data, seem to be in general agreement.

The D/H ratio has also been determined for Saturn and Uranus by Fink and Larsen (1978), Macy and Smith (1978), and Trafton and Ramsey (1980). The results are in modest agreement with the Jupiter values. As for Jupiter the determinations from HD are slightly higher than those from CH_3D. Tentative identifications of CH_3D in the atmosphere of Titan have been made by Lutz et al. (1981) and Gillett (1975). The two determinations for Uranus, from HD, are also in modest agreement with the Jovian values.

Assuming deuterium was originally homogeneously distributed in the solar nebula, the outer planets may still show variations in D/H due to

fractionation during planetary formation as predicted by Hubbard and MacFarlane (1980). However, they find that the value of D/H for Jupiter and for Saturn should both be similar to that of the protosolar nebula, independent of the individual formation processes. Therefore, the value of D/H in this paper should represent the best available value for the solar nebula, due mainly to the relatively unambiguous interpretation of the clear regions in the NEB.

An independent value of the protosolar D/H value can be estimated from He^3 in gas-rich meteorites and in the solar wind. Black (1971; 1972) has estimated $0.8\times10^{-5} < D/H < 3\times10^{-5}$ for the protosun from He^3 in gas rich meteorites. Geiss and Reeves (1972), and Geiss and Bochsler (1979) obtained $D/H = 2\text{-}2.5\times10^{-5}$ from the He^3/H ratio in the solar wind. Our value of $D/H = 3.6\ ^{+1.0}_{-1.4}\times10^{-5}$ is therefore in reasonable agreement with the value derived from He^3 in gas-rich meteorites and the solar wind. The close agreement implies the absence of fractionation in the solar nebula.

Many measurements of D/H exist for the interstellar medium, with the first identification of interstellar deuterium being in DCN in the Orion molecular cloud (Jefferts et al. 1973). The D/H values derived from the DCN/HCN ratio and from other deuterated molecules (DCO^+, NH_2D) are large and are difficult to evaluate quantitatively, due to chemical fractionation effects (Solomon and Woolf 1973). The most reliable value of interstellar D/H results from observations of the deterium and hydrogen Lyman lines in the line of sight to five early type stars, York and Rogerson, Jr. (1976) have determined $D/H = 1.8\pm0.4\times10^{-5}$. The D/H ratios inferred from the Lyman lines observations of Copernicus have been summarized by Laurent et al. (1979) and Bruston et al. (1981), indicating a mean value of $1.5\pm1.0\times10^{-5}$. Bruston et al. (1981) have reanalyzed the interstellar deuterium data, correcting for selective effects due to radiation pressure and UV photo-dissociation (from shielding of H_2), suggesting an unperturbed $D/H = 2.25\pm0.25\times10^{-5}$. The interstellar D/H values determined from the Lyman lines exhibit a significant spread, indicating innomogeneities in the interstellar medium and other uncertainties in the interpretation, such as the number of emitting clouds along the line of sight. As seen in Fig. 19, the interstellar D/H values tend to be slightly lower than those of the outer solar system and the protosolar nebula. This is in accordance with some deuterium depletion from stellar processing since the time of solar system formation.

The Big Bang is the most viable mechanism for producing deuterium (Epstein et al. 1976) and thus its abundance is of cosmological significance. The primordial D/H value is a sensitive parameter to the present day baryon density, which can be used to infer the matter density at the time of the Big Bang (Wagoner et al. 1973). The amount of deuterium presently observed can easily be produced with standard cosmological models of the Big Bang (Wagoner 1979; Wagoner et al. 1973; Wagoner et al. 1967). Although other non-cosmological mechanisms are capable of producing significant amounts of deuterium, such as shock waves, supernovae explosions, etc., none seems plausible or necessary (Epstein et al. 1976). The time evolution of D/H after synthesis in the Big Bang can be computed with models of chemical evolution in a galaxy. We have presented in Fig. 20 two evolutionary abundance curves (EAC) of deuterium from Audouze and Tinsley (1974). As an illustration of the sensitivity of D/H to the assumptions involved in galactic evolution models, two contrasting models are presented, the infall and the no infall model.

The infall model assumes extragalactic gas of primordial Big Bang composition enters the galaxy during its evolution at a rate of 2 percent of the total mass per 10^9 years. The no infall model does not assume an external flux of gas. In addition the infall model assumes intense star formation during the first 10^9 yr, transforming D rapidly to He^3, the D later is replenished from the primordial D in the infalling gas. The no infall model has a lower, more stretched out rate of star formation and the D is gradually destroyed through stellar processing.

Also shown on Fig. 20 are the observed D/H values for Jupiter from this investigation and for the protosolar nebula from Geiss and Bochsler (1979), for the time of solar system formation. The EAC curves have been normalized to pass through the center D/H value from this investigation. The observed values for the interstellar medium, corresponding in time to now, are shown from the summary of Bruston et al. (1981). Both galactic evolution models give agreement with the solar system formation D/H observations. However, the infall model predicts a higher D/H value than is presently observed and is thus excluded by observations. However, the infall model could be made consistent with observations for both time periods by varying the birthrate function or

the rate of infall. Thus the model of galactic evolution introduces some uncertainty in determining the value of primordial Big Bang D/H from solar system and interstellar medium observations. On the other hand, it should be possible in the future, with smaller uncertainties in the observations, to define better both the value of primordial and interstellar D/H and the models of galactic chemical evolution. Comparisons of the D/H observations to the galactic evolution model of Audouze and Tinsley (1974) which include the production of D in supernovae envelopes excludes the supernovae mechanism as a significant source of D.

Even with the large uncertainties in the observations and in the models, we can infer information concerning the present day baryon density. Using the IRIS D/H error bars, we extrapolate back in time to a range in primordial D/H ratio by number of $(5.8\text{-}8.1)\times10^{-5}$ for the no infall model and $(6.9\text{-}9.2)\times10^{-5}$ for the infall model. The primordial Big Bang D/H values have been converted to present day baryon density using Table 1 of Wagoner (1973); this relationship is illustrated on the left of Fig. 20. The range of present day baryon densities is $\sim2.0\text{-}2.4\times10^{-31}$ gm/cm^3 for the no infall model and $\sim1.8\text{-}2.2\times10^{-31}$ gm/cm^3 for the infall model. This range represents an upper limit for the present baryon density and leads to an open universe in the standard Big Bang models (Wagoner, 1973), a critical density of 4.5×10^{-30} gm/cm^3 and of 1.8×10^{-29} gm/cm^3 being required to close the Universe for a Hubble expansion parameter H_o of 50 and of 100 km sec^{-1} Mpc^{-1}, respectively (Epstein et al. 1976). This last value of H_o seems to be favored by recent determinations (de Vaucouleurs 1980).

If massive neutrinos dominate the Universe (Schramm and Steigman 1981), a question which is still open, the production of primordial deuterium would not be changed, in the Standard Model, and the present derivation of the baryon density is still valid, but the total density could be drastically higher and the Universe could be closed.

VIII. CONCLUSIONS

The Voyager IRIS measurements offer improvements in composition information over previous ground-based and airborne data because of high spatial resolution, which allows the selection of "cloud-free" regions within

the NEB, and because of the wide spectral range, which allows the retrieval of temperature structure and gas composition for the same volume element at the same time. Also the wide spectral range is more constraining on the altitude distributions of the gases with spectral features occurring in several regions throughout the 180-2250 cm^{-1} range (NH_3, PH_3 and CH_3D), than when only one narrow spectral region needs to be fit.

An average spectrum representing a very homogenous "cloud-free" region in the NEB has been constructed from 51 individual Voyager IRIS spectra of the clearest regions in the NEB. The average spectrum has been compared to synthetic spectra to derive gas composition information for altitudes corresponding to 0.2-5 bar. Altitude profiles have been derived for NH_3, PH_3, CH_3D, GeH_4, and H_2O. The retrieved profile for NH_3 is close to saturation in the .2-.4 bar range, then follows an increasing sub-saturation profile, reaching a depletion factor of $\sim$3 at .7 bar. In the .8-1 bar range the derived value is $^{q}NH_3 = 1.78 \pm .89 \times 10^{-4}$, in agreement with the solar value of Lambert (1978). The inferred NH_3 distribution for the NEB is in agreement with the concept of a belt being a downwelling region which is depleted in condensible gases. The PH_3 inferred distribution shows depletion in the .4-.7 bar range. Comparison to the semi-quantitative photochemical models of Strobel (1977) indicates best agreement with the model prediction for coupled NH_3-PH_3 photochemistry. The PH_3 abundance of the 1-4 bar region was $^{q}PH_3 = 6 \pm 2 \times 10^{-7}$ which is in agreement with the solar value of Cameron (1973). The mole fraction for CH_3D, determined from the 1120-1220 cm^{-1} and 2100-2200 cm^{-1} spectral ranges, was found to be $^{q}CH_3D = 3.5^{+1.0}_{-1.3} \times 10^{-7}$. The GeH_4 mole fraction of $7 \pm 2 \times 10^{-10}$ at the 2-5 bar level is a factor of 10 lower than the solar value. The H_2O mole fraction is $\sim 1 \times 10^{-6}$ at 2.5 bar increasing to $\sim 3 \times 10^{-5}$ at the 4 bar level. The IRIS inferred distributions for NH_3, PH_3, CH_3D, GeH_4 and H_2O probably represent the best values to date for the NEB, due to the relatively unambiguous interpretation from a homogenous relatively "cloud-free" region.

The determination of D/H for Jupiter has also been improved through the use of the more accurate values of $^{q}CH_3D$ and $^{q}CH_4$ inferred from the IRIS measurements. Our value of $D/H = 3.6^{+1.0}_{-1.4} \times 10^{-5}$ is in reasonable agreement and consistent with the D/H values derived from He^3 in gas-rich meteorites and the solar wind. If the Jovian atmospheric D/H value is representative of the bulk

planet the agreement with the meteoritic and solar wind values implies that Jupiter has retained its protosolar nebula value without fractionation during accretion.

The abundance of primordial deuterium formed in the standard Big Bang model is a sensitive indicator of the present baryon density of the Universe. Taking the IRIS value of D/H as representative of the solar nebula at the time of the solar system formation and correcting for the time evolution of D/H with the model for chemical evolution of the galaxy of Audouze and Tinsley (1974), a value of $5.5\text{-}9.0\times10^{-5}$ is obtained for the primordial D/H ratio. This ratio yields $1.8\text{-}2.4\times10^{-31}$ gm/cm^3 as an upper limit to the present day baryon density and leads to an open Universe in the standard Big Bang models (Wagoner 1973), provided that the mass of the universe is dominated by baryons.

The interpretation of the IRIS data is limited in many instances by a lack of knowledge in the basic molecular data. The most significant molecular shortcoming for investigations of the deep atmosphere of Jupiter is the far wing line shape arising from CH_4-H_2 and NH_3-H_2 collisions which strongly effects interpretation of all Jovian window measurements. The sensitivity of the continuum to the far wing line shape has been illustrated in this paper for the 1100-1200 window. The effect is even stronger in the 1800-2250 cm^{-1} window. Further advances in interpretation of the deep atmosphere of Jupiter from window measurements are contingent on improved knowledge of the CH_4-H_2 and NH_3-H_2 far wing line shape.

Acknowledgements

We wish to thank J. Schneider for a number of enlightening discussions on the Big Bang theory, and G. Tarrago and G. Poussique for providing us with CH_3D and PH_3 data before publication. We would also like to thank G. Bjoraker for helpful discussions on the 1900-2250 cm^{-1} region analysis and J. Tingley for his contributions in the synthetic modelling.

References

Atreya, S. K., Donahue, T. M., and Kuhn, W. R. 1977, Icarus, 31, 348.

Audouze, J., and Tinsley, B. M. 1974, Ap. J., 192, 487.

Baluteau, J. P., Marten, A., Bussoletti, E., Anderegg, M., Moorwood, A. F. M., Beckman, J. E., and Coron, N. 1978, Astron. & Astrophys., 64, 61.

Baluteau, J. P., Marten, A., Moorwood, A. F. M., Anderegg, M., Biraud, Y., Coron, N., and Gautier, D. 1980, Astron. & Astrophys., 81, 152.

Barshay, S. S., and Lewis, J. S. 1978, Icarus, 33, 593.

Beer, R., and Taylor, F. W. 1973, Ap. J., 179, 309.

Beer, R., and Taylor, F. W. 1978, Ap. J., 219, 763.

Beer, R., and Taylor, F. W. 1979, Icarus, 40, 189.

Birnbaum, G. 1979, J. Quant. Spectrosc. Radiat. Transfer, 21, 597.

Bjoraker, G., Fink, U., Larson, H. P., and Kunde, V. G. 1981, BAAS, 13, 735.

Black, D. C. 1971, Nature Phys. Sci., 234, 148.

Black, D. C. 1972, Geochimica et Cosmochimica Acta, 36, 347.

Black, D. C. 1973, Icarus, 19, 154.

Boato, G. 1954, Geochimica et Cosmochimica Acta, 6, 209.

Bruston, P., Audouze, J., Vidal-Madjar, A., and Laurent, C. 1981, Ap. J., 243, 161.

Cameron, A. G. W. 1973, Space Sci. Rev., 15, 121.

Combes, M., and Encrenaz, T. 1979, Icarus, 39, 1.

Combes, M., Courtin, R., Caldwell, J., Encrenaz, T., Fricke, K. H., Moore, V., Owen, T., and Butterworth, P. S. 1980, Advances in Space Research, Planetary Aeronomy and Astronomy, ed. S. K. Atreya and J. J. Caldwell.

Conrath, B. J., and Revah, I. 1972, Proc. Workshop on Mathematics of Profile Inversion, NASA TM-X-62150.

Conrath, B. J., and Gautier, D. 1979, Workshop on Interpretation of Remotely Sensed Data, Williamsburg, Va., May 23-25.

Craig, H. 1961, Science, 133, 1833.

De Vaucouleurs, G. 1980, Texas Symposium of Relativistic Astrophysics, Baltimore, MD.

Drossart, P., Encrenaz, T., Kunde, V., Hanel, R., and Combes, M. 1982, submitted to Icarus.

Encrenaz, T., Combes, M., and Zeau, Y. 1978, Astron. & Astrophys., 70, 19.

Encrenaz, T., Combes, M., and Zeau, Y. 1980, Astron. & Astrophys., 84, 148.

Encrenaz, T. and Combes, M. 1981, in IAU Symposium No. 96, Infrared Astronomy, ed. C. G. Wynn-Williams and D. P. Cruikshank.

Encrenaz, T., and Combes, M., 1982, preprint.

Epstein, R. I., Lattimer, J. M., and Schramm, D. N. 1976, Nature, 263, 198.

Erickson, E. F., Goorvitch, D., Simpson, J. P., and Stecker, D. W. 1978, Icarus, 35, 61.

Fink, U., and Larson, H. P. 1978, Science, 201, 343.

Fink, U., Larson, H. P., and Treffers, R. R. 1978, Icarus, 34, 344.

Gautier, D., Lacombe, A., and Revah, I. 1977, J. Atmos. Sci., 34, 1130.

Gautier, D., Marten, A., Baluteau, J. P., and Lacombe, A. 1979, Icarus, 37, 214.

Gautier, D., Conrath, B., Flasar, M., Hanel, R., Kunde, V., Chedin, A., and Scott, N. 1981, JGR, 86, 8713.

Gautier, D., Bezard, B., Marten, A., Baluteau, J. P., Scott, N., Chedin, A., Kunde, V., and Hanel, R. 1982, Ap. J., in press.

Geiss, J., and Bochsler, P. 1979, Proc. 4th Solar Wind Conference, Burghausen.

Geiss, J., and Reeves, H. 1972, Astron. & Astrophys., 18, 126.

Geiss, J., and Reeves, H. 1981, Astron. & Astrophys., 93, 189.

Gillett, F. C. 1975, Ap. J. (Letters), 201, L41.

Goorvitch, D., Erickson, E. F., Simpson, J. P., and Tokunaga, A. T. 1979, Icarus, 40, 75.

Hanel, R., Conrath, B., Flasar, M., Kunde, V., Lowman, P., Maguire, W., Pearl, J., Pirraglia, J., Samuelson, R., Gautier, D., Gierasch, P., Kumar, S., and Ponnamperuma, C. 1979, Science, 204, 972.

Hubbard, W. B., and MacFarlane, J. J. 1980, Icarus, 44, 676.

Jefferts, K. B., Penzias, A. A., and Wilson, R. W. 1973, Ap. J. (Letters), 179, L57.

Kolodny, Y., Kerridge, J. F., and Kaplan, I. R. 1980, Earth and Planetary Science Letters, 46, 149.

Kunde, V. G. 1982, Workshop on Vibrational Rotational Spectroscopy for Planetary Atmospheres, 17-19 March, 1980, Annapolis, MD.

Kunde, V. G., and Maguire, W. C. 1974, J. Quant. Spectrosc. Radiat. Transfer, 14, 803.

Lacy, J. H., Larabee, A. I., Wollman, E. R., Geballe, T. R., Townes, C. H., Bregman, J. D., and Rank, D. M. 1975, Ap. J. (Letters), 198, L145.

Lambert, D. 1978, Mon. Not. Roy. Astron. Soc., 82, 249.

Larson, H. P. 1977, Proceedings of Symposium on Planetary Atmospheres, Ottawa, Canada.

Larson, H. P., Fink, U., Treffers, R., and Gautier III, T. N. 1975, Ap. J. (Letters), 197, L137.

Larson, H. P., Treffers, R. R., and Fink, U. 1977, Ap. J., 211, 972.

Laurent, C., Vidal-Madjar, A., and York, D. G. 1979, Ap. J., 229, 923.

Lutz, B. L., De Berg, C., Maillard, J. P., Owen, T., and Brault, J. 1981, Ap. J. (Letters), 248, L141.

Macy, Jr., W. and Smith, W. H. 1978, Ap. J. (Letters), 222, L73.

Marten, A., Courtin, R., Gautier, D., and Lacombe, A., 1980, Icarus, 41, 410.

Marten, A., Rouan, D., Baluteau, J. P., Gautier, D., Conrath, B. J., Hanel, R., Kunde, V., Samuelson, R., Chedin, A., and Scott, N. 1981, Icarus, 46, 233.

McKellar, A. R. W., Goetz, W., and Ramsay, D. A. 1976, Ap. J., 207, 663.

Prinn, R. G., and Lewis, J. S. 1975, Science, 190, 274.

Ridgway, S. T., Larson, H. P., and Fink, U. 1976a, In "Jupiter", T. Gehrels, ed., p. 384, University of Arizona Press, Tucson, Arizona.

Ridgway, S. T., Wallace, L., and Smith, G. R. 1976b, Ap. J., 207, 1002.

Robert, F., Merlivat, L., and Javoy, M. 1977, Meteoritics, 12, 349.

Robert, F., Merlivat, L., and Javoy, M. 1978, Meteoritics, 13, 613.

Robert, F., Merlivat, L., and Javoy, M. 1979, Nature, 282, 785.

Schramm, D. N., and Wagoner, R. V. 1974, Physics Today, 27, 41.

Schramm, D. N., and Steigman, G., 1981, Gen. Rel. Grav. (in press).

Scott, N. A., 1973, J. Quant. Spectrosc. Radiat. Transfer, 14, 691.

Scott, N. A., and Chedin, A. 1981, J. of Applied Meteorology (in press).

Smith, W. L. 1970, Applied Optics, 9, 1993.

Solomon, P. M., and Woolf, N. J. 1973, Ap. J. (Letters), 180, L89.

Strobel, D. F. 1977, Ap. J. (Letters), 214, L97.

Terrile, R. J., Capps, R. W., Backman, D. E., Becklin, E. F., Cruikshank, D. P., Berchman, C. A., and Brown, R. H. 1979, Science, 204, 1007.

Tokunaga, A. T., Knacke, R. F., Ridgway, S. T., and Wallace, L. 1979, Astrophys. J., 232, 603.

Tokunaga, A. T., Knacke, R. F., and Ridgway, S. T. 1981, Icarus, 44, 93.

Trafton, L., and Ramsay, D. A. 1980, Icarus, 423.

Trauger, J. T., Roesler, F. L., Carleton, N. P., and Traub, W. A. 1973, Ap. J. (Letters), 184, L137.

Trauger, J. T., Roesler, F. L., and Mickelson, M. E. 1977, B.A.A.S., 9, 516.

Wagoner, R. V. 1973, Ap. J., 179, 343.

Wagoner, R. V. 1979, Physical Cosmology, ed. by Balian, R., Audouze, J., and Schramm, D. N., North-Holland Publishing Company, New York, New York, p. 395.

Wagoner, R. V., Fowler, W. A., and Hoyle, F. 1967, Ap. J., 148, 3.

Wallace, L., and Hunten, D. M. 1978, Reviews of Geophysics and Space Physics, 16, 289.

Weidenschilling, S. J., and Lewis, J. S. 1973, Icarus, 20, 465.

Winters, B. H., Silverman, S., and Benedict, W. S. 1964, J. Quant. Spectrosc. Radiat. Transfer, 4, 527.

York, D. G., and Rogerson, Jr., J. B. 1976, Ap. J., 203, 378.

APPENDIX A. SUMMARY OF MOLECULAR PARAMETERS

A summary of the important molecular parameters for the strongest absorption bands is given in Table A1.

The determination of the H_2 absorption coefficient is based on the laboratory and theoretical work of Birnbaum and Cohen (1976), Birnbaum (1978), and Cohen and Birnbaum (1981). The absorption lines for the ν_4 bands of $^{12}CH_4$ and $^{13}CH_4$ are from the GEISA spectral line parameter compilation (Chedin et al. 1981). Spectroscopic data of the ν_4 band of methane is from Orton and Robiette (1980). The $^{12}CH_4$ band intensity is from Chedin et al. (1978), the terrestrial ratio of 89 was assumed for the $^{12}CH_4/^{13}CH_4$ ratio. The pressure broadened half-widths were taken as .075 and .045 cm^{-1} for CH_4-H_2 and CH_4-He collisions, respectively (Varanasi and Tejwani, 1972). The absorption lines for CH_3D are from the GEISA line parameters compilation (Chedin et al. 1980). The molecular parameters for the ν_2 CH_3D band have been generated using symmetric rotor theory (Allen and Cross, 1963; Allen and Plyler, 1959). The band intensity for this band is based on the multiplet analysis of lines by Sarangi and Varanasi (1975). The half-widths were assumed to be the same as for CH_4.

The molecular line parameters for the $^{14}NH_3$ and $^{15}NH_3$ bands have been generated by Husson et al. (1979) from standard pyramidal XY_3 formulation. The pure rotation transitions in the ground state, and the rotation-inversion transition in the ν_2 and $2\nu_2$ levels of $^{14}NH_3$ have been reinvestigated by Husson et al. (1981). The band intensity adopted for the rotational NH_3 band was from Husson, et al. (1981), and for the ν_2 bands from Taylor (1973). The ν_4 band at 1627 cm^{-1} was computed from the work of Curtis (1974) with the band intensity from McKean and Schatz (1956). The $2\nu_2^s$ band intensity was normalized to be consistent with the Voyager IRIS spectrum for a solar NH_3 mixing ratio of 1.78×10^{-4}. This derived intensity represents a lower limit to the true band intensity. The hydrogen broadened half-width was assumed to be .075 cm^{-1} (Varanasi, 1972) with the helium broadened value being .025 cm^{-1} (Berge and Gulkis, 1976).

Spectral line parameters for PH_3 were adopted from Tarrago et al. (1981) for ν_2 and ν_4, from Goldman (1979) for ν_1 and ν_3, and from Goldman (1980) for

tne 1925-2160 cm^{-1} region. The ν_2, ν_4, ν_1 and ν_3 band intensities are from McKean and Schatz (1956) and the 1925-2160 cm^{-1} band intensity is from Goldman (1980). As no experimental values are available, the PH_3 half-widths were taken to be the same as those of NH_3. The H_2O line parameters are from the AFCRL Atmospheric Absorption Line Parameters Compilation (McClatchey, et al., 1973) with the half-width values from the microwave measurements of the 22 GHz H_2O line (Liebe and Dillon, 1969).

The GeH_4 molecular parameters have been generated for the ν_3-band by using spherical top theory for triply-degenerate fundamentals. The rotational constants are from Lepage et al. (1976) and the band intensity is based on Fink, et al. (1978); the line half-widths are from Corice (1972).

References

Allen, H. C., and Cross, P. C. 1963, Molecular Vib-rotors (John Wiley and Sons, New York, New York).

Allen, Jr., H. C., and Plyler, E. K. 1959, J. Res. NBS, 63A, 145.

Berge, G. L., and Gulkis, S. 1976, in "Jupiter", T. Gehrels, ed., p. 621, University of Arizona Press, Tucson, Arizona.

Birnbaum, G. 1978, J. Quant. Spectrosc. Radiat. Transfer, 19, 51.

Birnbaum, G., and Cohen, E. R. 1976, Canad. J. Phys., 54, 593.

Chedin, A., Husson, N., Scott, N. A. and Gautier, D. 1978, J. Mol. Spectrosc., 71, 343.

Chedin, A., Husson, N., Scott, N. A., Cohen-Halluleh, I., and Berroir, A., 1981, Internal Reports 108 and 113, LMD, Ecole Polytechnique, Palaiseau, France.

Cohen, E. R., and Birnbaum, G. 1981, National Bureau of Standards report NBSIR 80-2175(R), National Bureau of Standards, Washington, D.C. 20234.

Corice, Jr., R. J., Fox, K., and Fletcher, W. H. 1972, J. Mol. Spectrosc., 41, 95.

Curtis, J. 1974, Dissertation, Ohio State University.

Fink, U., Larson, H. P., and Treffers, R. R. 1978, Icarus, 34, 344.

Goldman, A. 1979, Semi-annual report, 21 June, 1979, University of Denver, Denver, CO 80208.

Goldman, A. 1980, Semi-annual report, 30 June, 1980, University of Denver, Denver, CO 80208.

Husson, N., Chedin, A., and Scott, N. A. 1979, Internal report n° 90, L.M.D., Ecole Polytechnique, Palaiseau, France.

Husson, N., Goldman, A., and Orton, G. 1981, Preprint.

Lepage, P., Bregier, R., and Saint-Loup, R. 1976, Compt. Rend. B, 283, 179.

Liebe, H. J., and Dillon, T. A. 1969, J. Chem. Phys., 50, 727.

McClatchey, R. A., Benedict, W. S., Clough, S. A., Burch, D. E., Calfee, R. F., Fox, K., Rothman, L. S., and Garing, J. S. 1973, AFCRL-TR-73-0096.

McKean, D. C., and Schatz, P. N. 1956, J. Chem. Phys., 24, 316.

Orton, G. S., and Robiette, A. G. 1980, J. Quant. Spectrosc. Radiat. Transfer, 24, 81.

Sarangi, S., and Varanasi, P. 1975, J. Quant. Spectrosc. Radiat. Transfer, 15, 291.

Tarrago, G., Dang-Nhu, M., and Goldman, A. 1981, J. Mol. Spect., 88, 311.

Taylor, F. W. 1973, J. Quant. Spectrosc. Radiat. Transfer, 13, 1181. ERRATUM (1974). J. Quant. Spectrosc. Radiat. Transfer, 14, 547.

Varanasi, P. 1972, J. Quant. Spectrosc. Radiat. Transfer, 12, 1283.

Varanasi, P., and Tejwani, G. D. T. 1972, J. Quant. Spectrosc. Radiat. Transfer, 12, 849.

Table 1. Error Estimates for Inferred NH_3 Distribution

Pressure Level (Range)	Evaluation Wave Number	Mole Fraction	Random Error		*Systematic Error			*Total Error
(bar)	(cm^{-1})	q	ΔT_I (K)	$\Delta q_r'$	Δq_1	Δq_2	Δq_3	Δq
.3 (.14-.4)	967	1.4×10^{-6}	.8	±.6*	±.01	± .14	±.07	±0.6
.45 (.25-.65)	970	8.9×10^{-6}	.5	±.5	±.09	± .89	±.45	±1.1
.6 (.4-.8)	980	3.0×10^{-5}	.2	±.3	±.03	± .30	±.15	±0.4

*The error estimates should be multiplied by the same exponential factor as the mole fraction for that level.

Table 2. Summary of Observed Ratios of D/H

Determination	Relevant Time Period	D/H_5 ($*10^{-5}$)	Reference
EARTH			
a) Deep ocean HDO	Solar System Formation	15.8±2	Craig, 1961
JUPITER			
b) Atmospheric CH_3D	"	$2.0^{+1.1}_{-0.8}$	*Beer & Taylor, 1973
c) " "	"	$3.0^{+1.8}_{-1.2}$	*Beer & Taylor, 1978
d) " "	"	<1.9	*Encrenaz et al., 1980
e) " "	"	$3.6^{+1.0}_{-1.4}$	*This investigation
f) Atmospheric HD	"	5.6±1.4	Trauger et al., 1973 McKellar et al., 1976
g) " "	"	5.1±0.7	Trauger et al., 1977
h) " "	"	1.0-2.6	*Combes & Encrenaz, 1979
SATURN			
i) Atmosphere HD	"	5.1±0.7	Trauger et al., 1977
j) Atmospheric CH_3D	"	$2.0^{+2.0}_{-1.0}$	Fink & Larson, 1978
k) Atmospheric HD	"	5.5±2.9	Macy and Smith, 1978
URANUS			
l) Atmospheric HD	"	3.0±1.2	Macy and Smith, 1978
m) " "	"	4.8±1.5	Trafton & Ramsey, 1980
PROTOSOLAR NEBULA			
n) Meteoritic He^3	"	0.8-3	Black, 1971, 1972
o) Solar wind He^3	"	2.5±0.5	Geiss & Reeves, 1972
p) Solar wind He^3	"	$2.0^{+1.5}_{-1.0}$	Geiss & Bochsler, 1979
INTERSTELLAR MEDIUM			
q) D Lyman lines from Copernicus	Now	1.8±0.4	York & Rogerson, 1976
r) Summary of D/H observations	"	1.5±1.0	Bruston et al., 1981
s) Re-analysis of D/H observations	"	2.25±0.25	Bruston et al., 1981

*These Jovian D/H values have been computed or recomputed with C/H = 2.07 * solar (Gautier et al., 1982), yielding CH_4/total = 1.75×10^{-3}.

Table A1. Summary of Molecular Data for Strongest Absorption Bands

Gas	Band Center (cm^{-1})	Band Designation	Band Intensity ($cm \cdot molec^{-1}$) (296K)	Band Intensity (cm^{-2} atm^{-1}) (STP)	Band Intensity (cm^{-2} atm^{-1}) (300K)	α ($X-H_2$) (cm^{-1}/atm)	α ($X-He$) (cm^{-1}/atm)
CH_4:	1304	ν_4	5.72×10^{-18}	153.8	140.0	.075	.045
CH_3D:	1161	ν_6	2.45 "	65.9	60.0	.075	.045
	1307	ν_3	1.84 "	49.4	45.0	"	"
	---	ν_5	.61 "	16.5	15.0	"	"
	2200	ν_2	1.04 "	27.9	25.4	"	"
NH_3:	50-250	Rotational	18.1 "	486.3	442.8	.075	.025
	629	$2\nu_2^s - \nu_2^a$	1.49 "	4.0	3.6	"	"
	932, 968	ν_2	21.6 "	580.9	528.9	"	"
	950	$2\nu_2^a - 2\nu_2^s$	.089 "	2.4	2.2	"	"
	1627	ν_4	4.50 "	120.8	110.0	"	"
	1882	$2\nu_2^s$	.0007 "	0.02	0.02	"	"
PH_3:	992	ν_2	3.35 "	90.1	82.0	"	"
	1118	ν_4	4.17 "	112.0	102.0	"	"
	1925-2160	-	.13 "	3.6	3.3	"	"
	2311	ν_1	10.63 "	285.6	260.0	"	"
	2320	ν_3	10.63 "	285.6	260.0	"	"
H_2O:	1595	ν_2	10.6 "	285.1	259.6	.084	.025
GeH_4:	2112	ν_3	45.0 "	1208.1	1100	.075	.045

Figure Captions

Fig. 1. Observed thermal emission spectrum for the clearest region of the NEB between 180 and 1500 cm^{-1}. This spectrum is an average of 51 individual spectra. The spectral features observed for the gases H_2, NH_3, PH_3 and CH_3D are of tropospheric and C_2H_2 is of stratospheric origin. CH_4 is well-mixed through both regions. The small standard deviation in brightness temperature, shown in the lower panel, indicates the average spectrum represents a very homogenous region of the NEB.

Fig. 2. Observed thermal emission spectrum for the clearest region of the NEB between 1800 and 2250 cm^{-1}. This spectrum is an average of 51 individual spectra. The spectral features observed for the gases NH_3, H_2O, GeH_4, CH_3D, and PH_3 originate at 1-5 bar. The small standard deviation in brightness temperature, shown in the lower panel, indicates the average spectrum represents a very homogenous region of the NEB.

Fig. 3. Atmospheric pressure levels where the optical depth equals unity for the 0-1400 cm^{-1} region. The maximum contribution to the emergent radiation originates from this level.

Fig. 4. Same as Fig. 3, except for 1825-2225 cm^{-1} region.

Fig. 5. Temperature structure for the NEB. The solid line represents the temperature profile obtained by inversion of the NEB spectral radiances within the S(0) and S(1) H_2 lines and the 1306 cm^{-1} band of CH_4. The dashed line is an extrapolation from 0.8 bar to deeper levels along a 2.1 K/km adiabat. The theoretical cloud layers of Weidenschilling and Lewis (1973) are indicated schematically on the left.

Fig. 6. Synthetic homogenous path spectra for the gases in the Jovian atmosphere absorbing in the 850-1300 cm^{-1} region. The transmittances were computed for the average temperature (125K) and pressure

(.4 bar), and the optical pathlength (U in cm atm at NTP) down to the .8 bar level. For NH_3 in b) the 850-1125 cm^{-1} region is saturated for u = 30 cm atm. To illustrate the NH_3 line structure in this region, the transmittance for u = 10 cm atm (corresponding to the .5 bar level) is also included, and it is this curve which is included in the composite in e). The composite spectrum in e) illustrates the strong overlapping and blending of these gases at the IRIS 4.3 cm^{-1} resolution.

Fig. 7. Comparison of observed and synthetic spectrum for the 180-300 cm^{-1} region. The a) panel illustrates the effect of the NH_3 distribution on the emergent brightness temperature spectrum in the .2 to .9 bar altitude range. The b) panel illustrates the effect of the NH_3 distribution in the well-mixed region (P > .8 bar) on the emergent brightness temperature spectrum, with the solar value of $^qNH_3$ being 1.8×10^{-4} (Lambert, 1978). The spectrum is sensitive to NH_3 in the well-mixed region only in the continua between the absorption lines. The 0.5 solar curve in the 210 cm^{-1} region is obscured by the observed spectrum. The instrument noise level in the observed spectrum is $\sim$ 0.03 K.

Fig. 8. Comparison of observed and synthetic spectra for the 850-1100 cm^{-1} region. The best agreement with the observed spectrum is obtained with the inferred NH_3 profile (Fig. 16). Absorption by PH_3 was included using its inferred distribution. The instrument noise level in the observed spectrum is indicated by the small vertical error bars.

Fig. 9. Synthetic spectra for the 1100-1250 cm^{-1} region. Absorption by NH_3, CH_4, PH_3, and CH_3D was included using their inferred distribution. The strong effect of the far wing line shape on the location of the continuum is illustrated for two values of the "cut-off" of the Lorentz line shape. The large uncertainty in the far wing line shape, especially for CH_4-H_2 and NH_3-H_2 collisions, is the dominant error source for inferring gas composition from this spectral region.

Fig. 10. Comparison of observed and synthetic spectra to determine $^{q}CH_3D$ from the 1120-1220 cm^{-1} region. Absorption by NH_3, CH_4 and PH_3 was included using their inferred distributions. The uppermost curve has been computed including only the continuum absorption of H_2 and He, and the line absorption of CH_3D to assist in the location of CH_3D features in the observed spectrum. No unique CH_3D lines, including the Q-branch at 1156 cm^{-1}, can be identified in the observed spectrum, thus the $^{q}CH_3D$ determination depends on matching the observed and synthetic continua. The instrument noise level is indicated by the small vertical bars.

Fig. 11. Comparison of observed and synthetic spectra to determine $^{q}PH_3$ from the 1080-1180 cm^{-1} region. The PH_3 distributions are shown in Fig. 17. Absorption by NH_3, CH_4, and CH_3D was included using their inferred distributions. The uppermost curve has been computed, including only the continuum absorption of H_2 and He, and the line absorption of PH_3 to assist in the location of PH_3 features in the observed spectrum. Four of the PH_3 multiplets used in the analysis are indicated by the vertical cross-hatched regions. The instrument noise level is indicated by the small vertical bars.

Fig. 12. Synthetic homogenous path spectra for the gases in the Jovian atmosphere in the 1800-2250 cm^{-1} region. The transmittances were computed for the average temperature (200K) and pressure (1.25 bar), and the optical pathlength (U in cm atm at NTP) down to the 2.5 bar level in the Jovian atmosphere. The composite spectrum in f) illustrates the strong overlapping and blending of the gases at the IRIS 4.3 cm^{-1} resolution.

Fig. 13. Comparison of observed and synthetic spectra to determine $^{q}PH_3$ from the 2050-2225 cm^{-1} region. Absorption by NH_3, H_2O, GeH_4, and CH_3D was included using their inferred distributions. The uppermost curve has been computed including only the continuum absorption of H_2, He, CH_4 and the aerosol, and the line absorption of PH_3 to assist in the location of PH_3 features in the observed spectrum. The mole fraction of PH_3 is determined from the line to continuum ratio for multiplets

(3) and (4), and the continuum roll-off from 2170 to 2225 cm^{-1}. The instrument noise level is indicated by the small vertical bars underlying the spectra.

Fig. 14. Comparison of observed and synthetic spectra to determine $^{9}CH_3D$ from the 2050-2225 cm^{-1} region. Absorption by NH_3, H_2O, GeH_4, and PH_3 was included using their inferred distributions. The uppermost curve has been computed including only the continuum absorption of H_2, He, CH_4, aerosol, and the line absorption of CH_3D to assist in the location of CH_3D features in the observed spectrum. The mole fraction of CH_3D is determined from the line to continuum ratio for P branch multiplets (1) through (4) and the Q branch (5). The instrument noise level is indicated by the small vertical bars underlying the spectra.

Fig. 15. a) Comparison of observed and synthetic spectra for the 1800-2250 cm^{-1} region. The mole fraction of H_2O has been determined from the 1875-2100 cm^{-1} region using the six H_2O multiplets indicated. Absorption by NH_3, PH_3, GeH_4, and CH_3D was included using their inferred distributions. b) The effect of the well-mixed grey haze is illustrated. The optical depth of the haze is 0.54 at 5 bar (279K).

Fig. 16. Altitude profiles for gaseous NH_3 in the NEB. The inferred distribution, which gives the best fit to the IRIS spectrum, is sub-saturated in the upper troposphere. Below 1 bar region, agreement is found with the solar value of Lambert (1978). The NEB distribution from Tokunaga et al. (1980) was derived from ground-based infrared measurement. The spatially resolved IUE distribution corresponds to the Equatorial Zone, not the NEB. The model atmosphere predictions of Atreya et al. (1977) are included to illustrate the capability of one dimensional atmosphere photochemical models to explain the observed distributions. A quantitative comparison between the observed and model distributions should not be made, as the globally averaged model distributions are not appropriate for the spatially resolved NEB.

Fig. 17. Altitude profiles for gaseous PH_3 in the NEB. The inferred distribution represents the best fit to the IRIS spectrum. Distributions 1 and 2 are photochemical model predictions of Strobel (1977) normalized in the deep atmosphere to the value of $^{q}PH_3 = 6x10^{-7}$ determined in this investigation. Distribution 1 represents the PH_3 photochemical model of Prinn and Lewis (1976). Distribution 2 includes the coupled photochemistry of NH_3 and PH_3.

Fig. 18. The mole fraction of CH_3D as determined from the ν_6 band (1100-1200 cm^{-1}) at .6 bar and from the ν_2 band (2100-2225 cm^{-1}) at ~3 bar. The adopted curve represents the best value of $^{q}CH_3D$ as determined from this investigation.

Fig. 19. Comparison of D/H ratio determinations for solar system objects and the interstellar medium. The shaded area is defined from the 1 σ error bars from this investigation. The IRIS value of D/H is adopted as the best value for Jupiter, and, assuming Jupiter has retained its primordial abundance, as the most representative value of the protosolar nebula. See Table 2 for letters (a) through (s).

Fig. 20. Evolutionary abundance curve (EAC) for D/H. The effect of galactic chemical evolution on the D/H ratio is illustrated by two contrasting models of Audouze and Tinsley (1974). The EAC curves have been normalized to pass through the central D/H value from this investigation. The EAC curves have been used to determine the primordial D/H ratio, and subsequently the present day baryon density. The IRIS determined present day baryon densities are consistent with an open universe for either of the galactic evolution models.

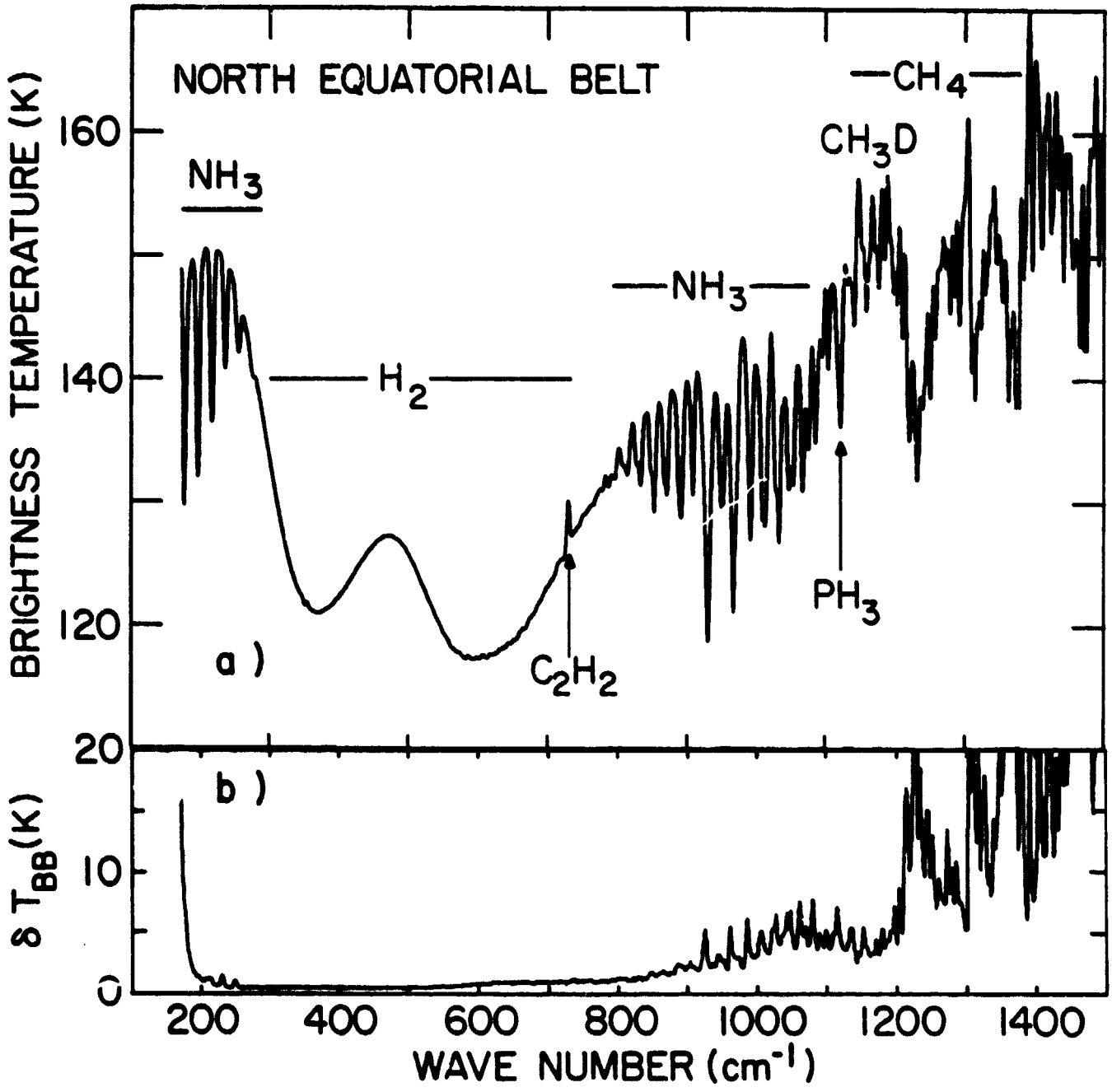
NORTH EQUATORIAL BELT
BRIGHTNESS TEMPERATURE (K)
160
140
120
NH3
H2
NH3
CH4
CH3D
PH3
C2H2
a)
b)
δ TBB (K)
20
10
0
200
400
600
800
1000
1200
1400
WAVE NUMBER (cm-1)

FIGURE 1

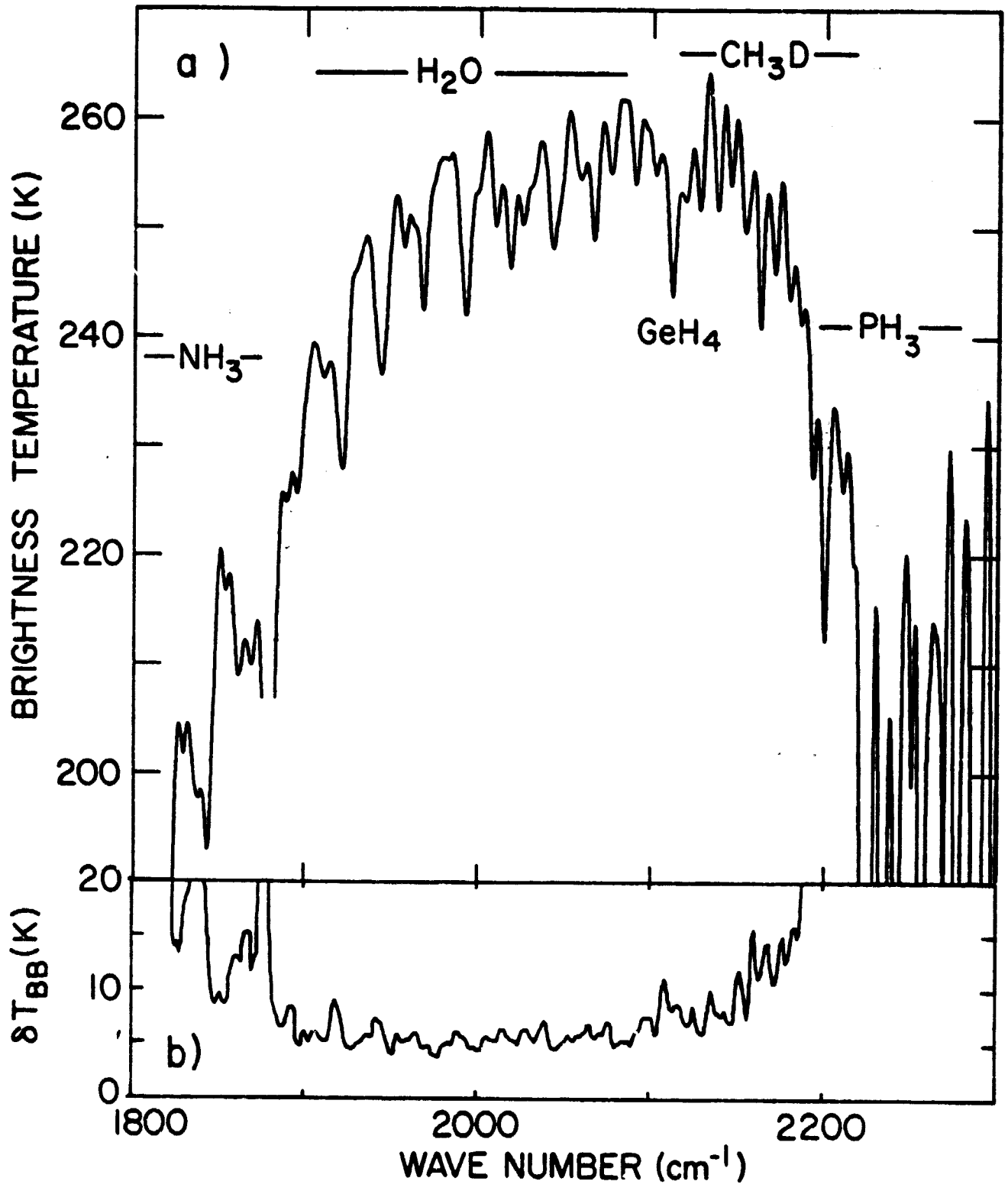
a)
H_2O
CH_3D
NH_3
GeH_4
PH_3
260
240
220
200
20
10
0
BRIGHTNESS TEMPERATURE (K)
δT_{BB}(K)
b)
1800
2000
2200
WAVE NUMBER (cm^{-1})

FIGURE 2

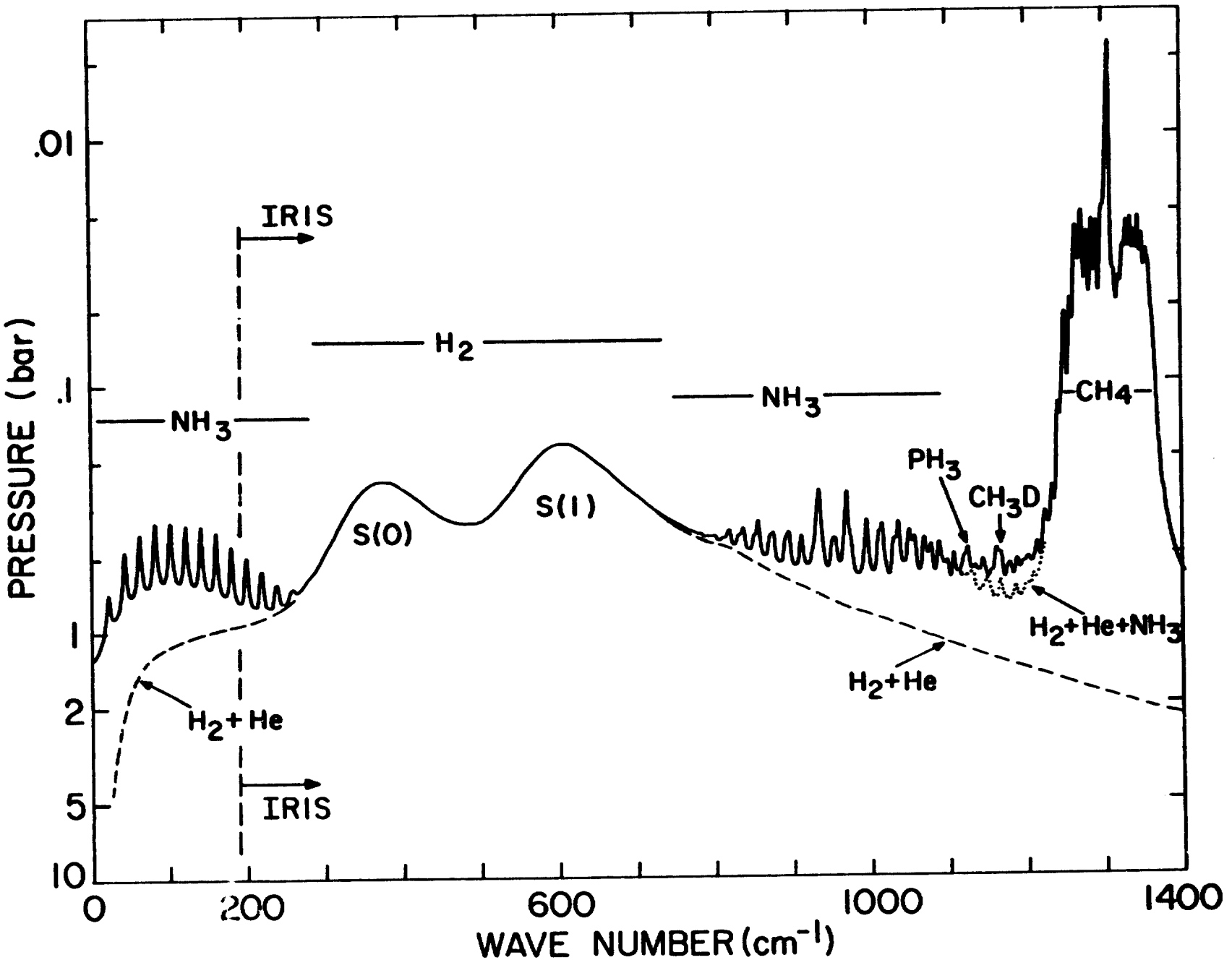
.01
.1
1
2
5
10
PRESSURE (bar)
IRIS
H_2
NH_3
NH_3
CH_4
PH_3
CH_3D
S(0)
S(1)
H_2+He+NH_3
H_2+He
H_2+He
IRIS
0
200
600
1000
1400
WAVE NUMBER (cm^{-1})

FIGURE 3

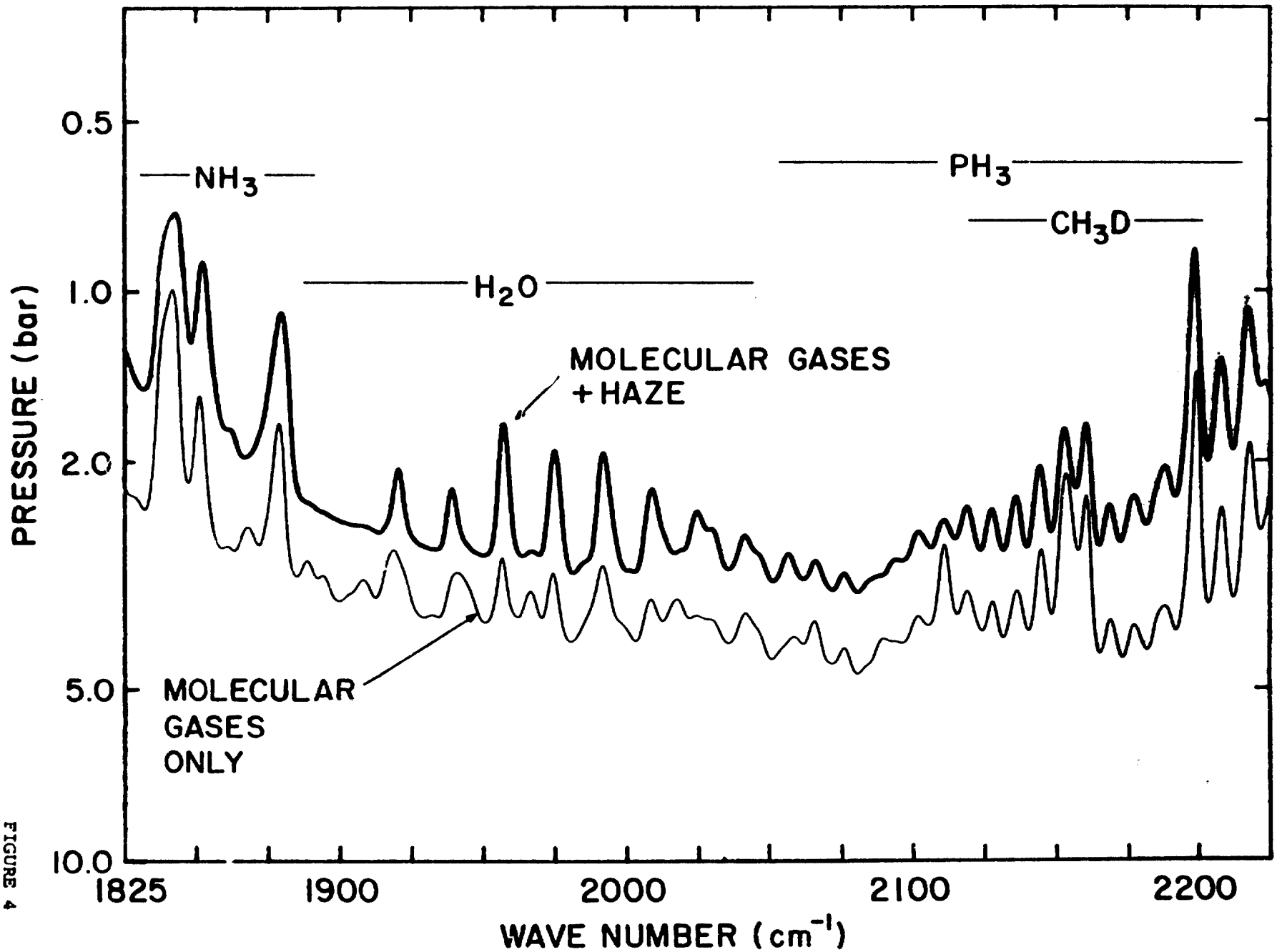
0.5
1.0
2.0
5.0
10.0
PRESSURE (bar)
NH3
H2O
PH3
CH3D
MOLECULAR GASES
+HAZE
MOLECULAR
GASES
ONLY
1825
1900
2000
2100
2200
WAVE NUMBER (cm-1)

FIGURE 4

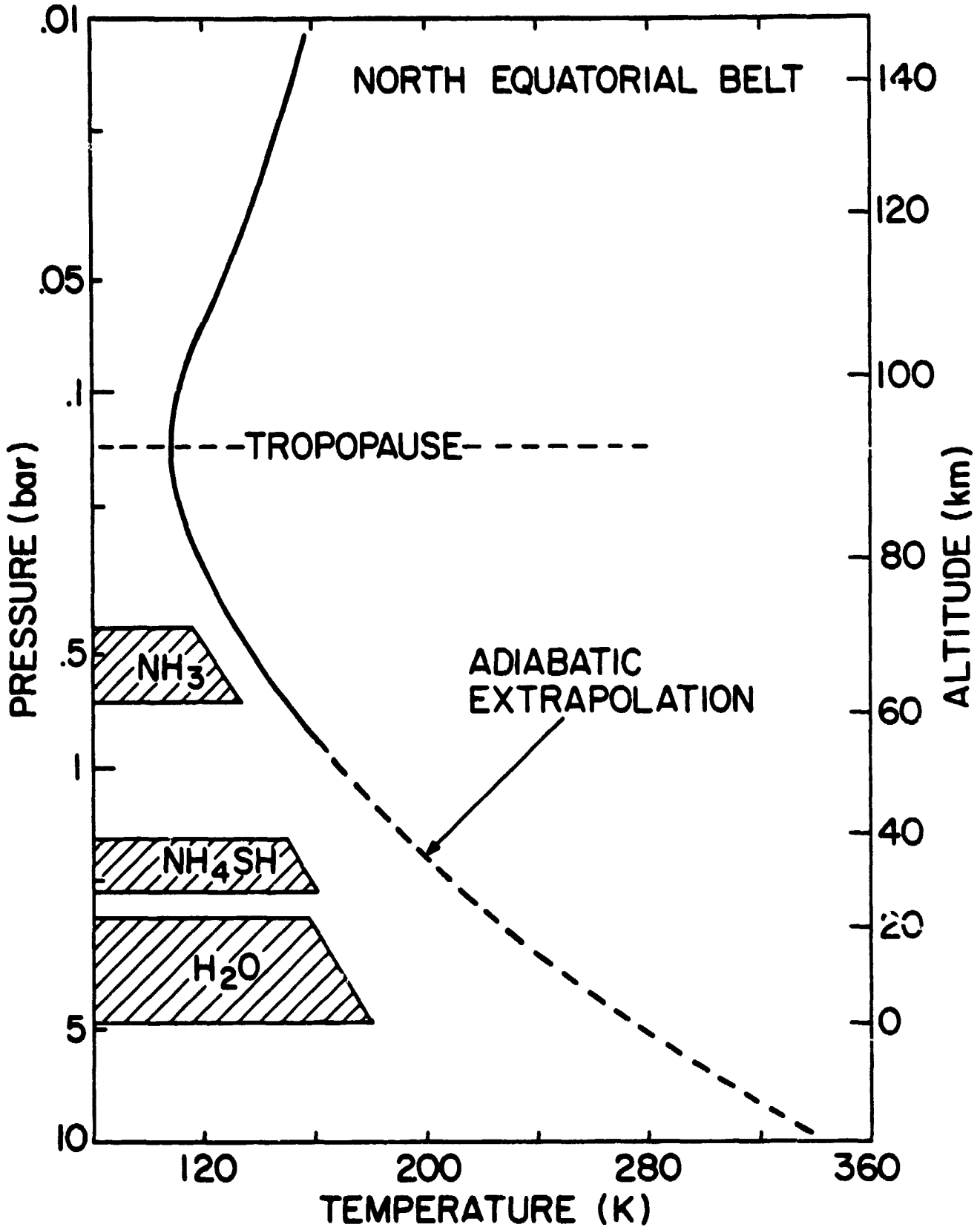
.01
.05
.1
.5
1
5
10
PRESSURE (bar)
NORTH EQUATORIAL BELT
TROPOPAUSE
NH3
NH4SH
H2O
ADIABATIC
EXTRAPOLATION
120
200
280
360
TEMPERATURE (K)
140
120
100
80
60
40
20
0
ALTITUDE (km)

FIGURE 5

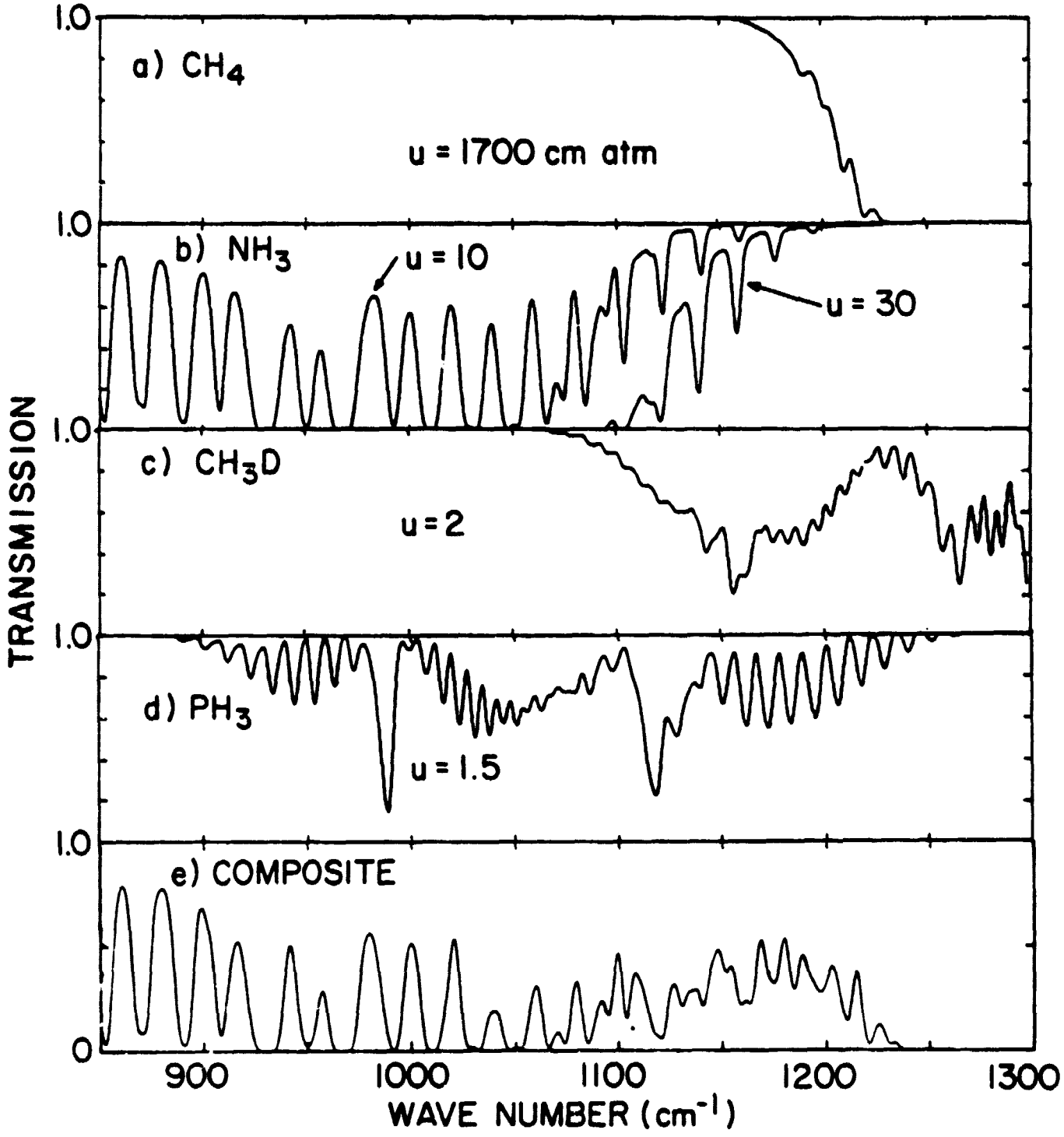
1.0
a) CH_4
u = 1700 cm atm
1.0
b) NH_3
u = 10
u = 30
1.0
c) CH_3D
u = 2
1.0
d) PH_3
u = 1.5
1.0
e) COMPOSITE
0
TRANSMISSION
900
1000
1100
1200
1300
WAVE NUMBER (cm^{-1})

FIGURE 6

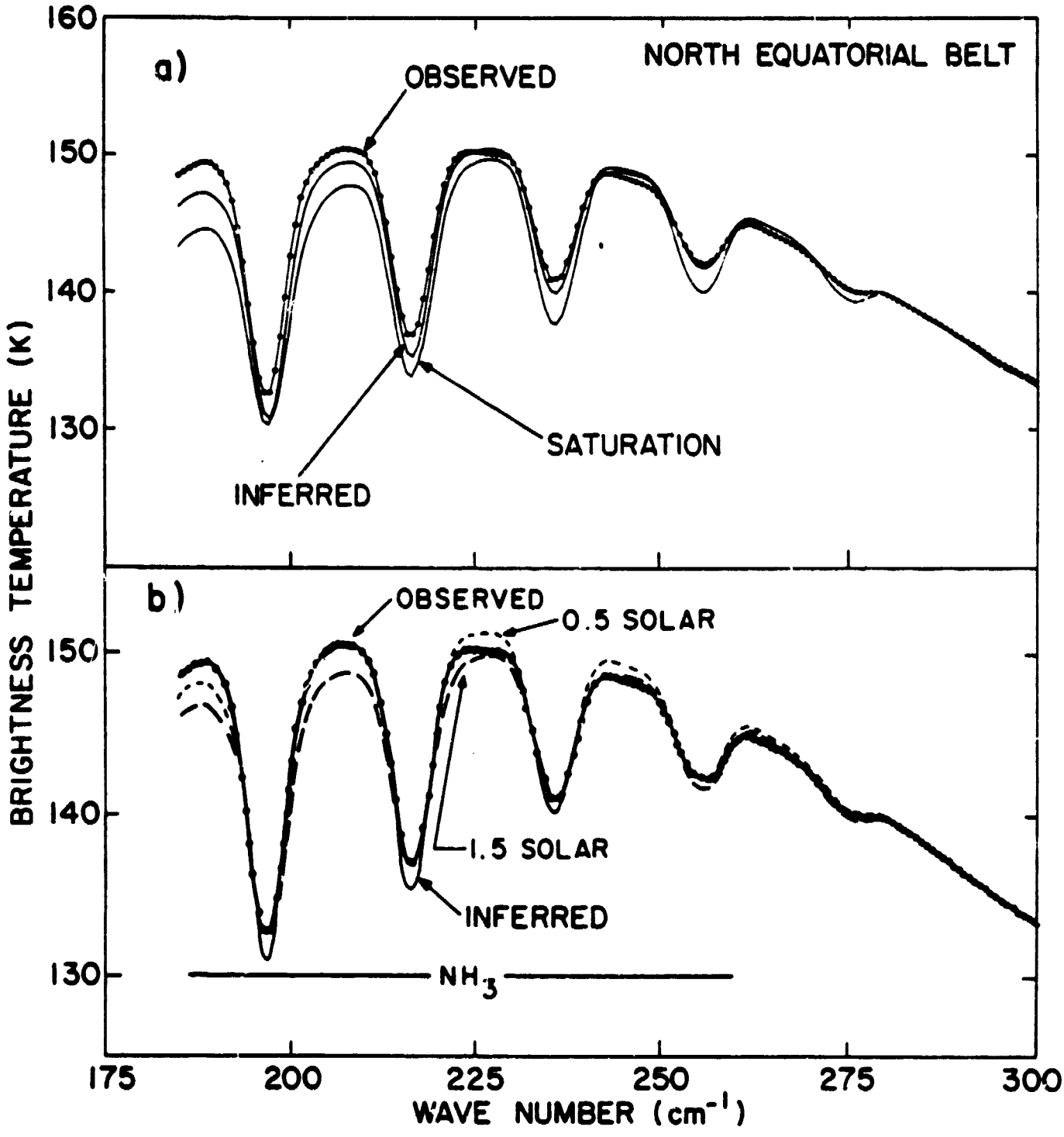
a)
NORTH EQUATORIAL BELT
OBSERVED
SATURATION
INFERRED
b)
OBSERVED
0.5 SOLAR
1.5 SOLAR
INFERRED
NH3
BRIGHTNESS TEMPERATURE (K)
160
150
140
130
150
140
130
175
200
225
250
275
300
WAVE NUMBER (cm-1)

FIGURE 7

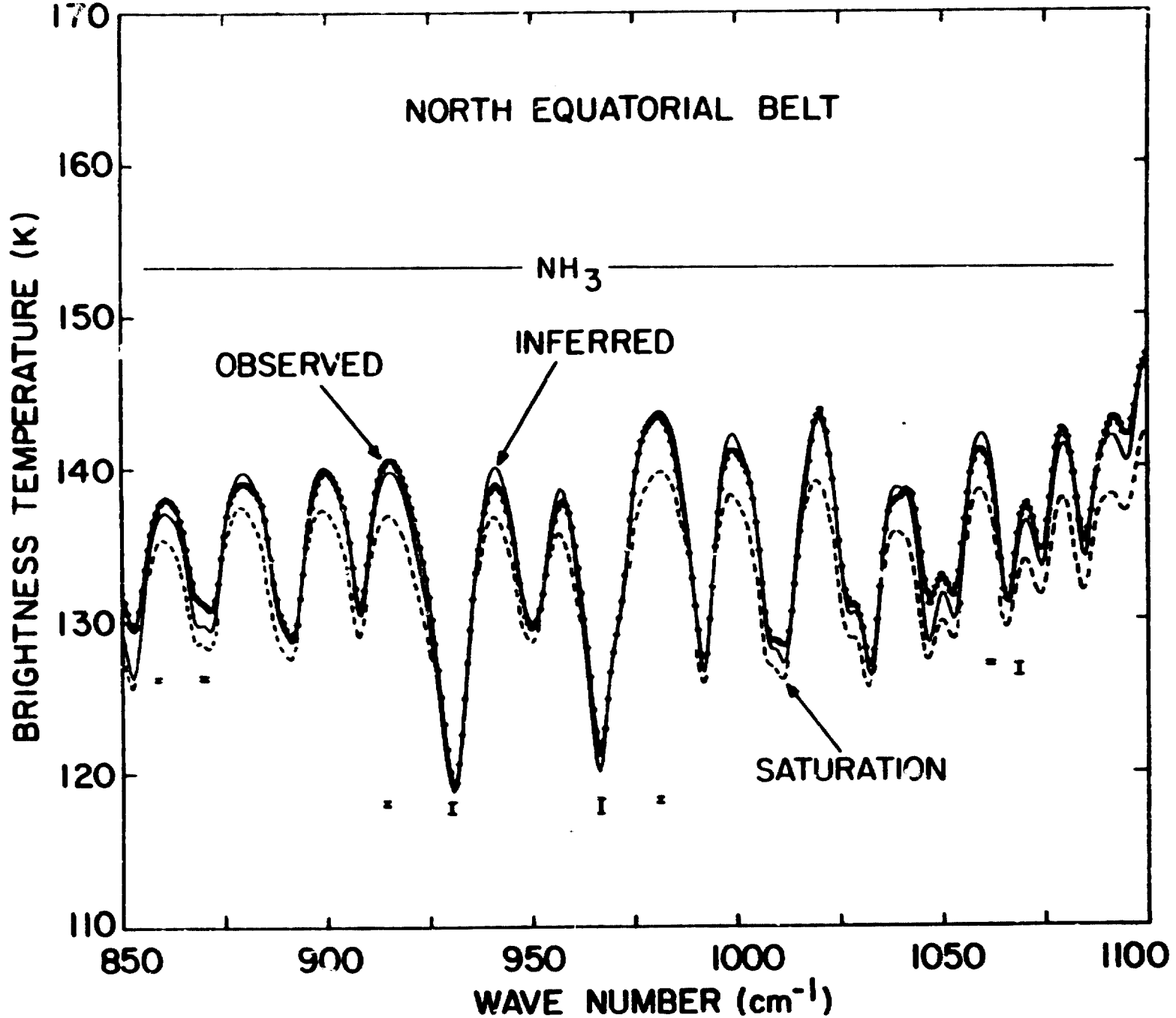
NORTH EQUATORIAL BELT
NH3
OBSERVED
INFERRED
SATURATION
BRIGHTNESS TEMPERATURE (K)
WAVE NUMBER (cm-1)
170
160
150
140
130
120
110
850
900
950
1000
1050
1100

FIGURE 8

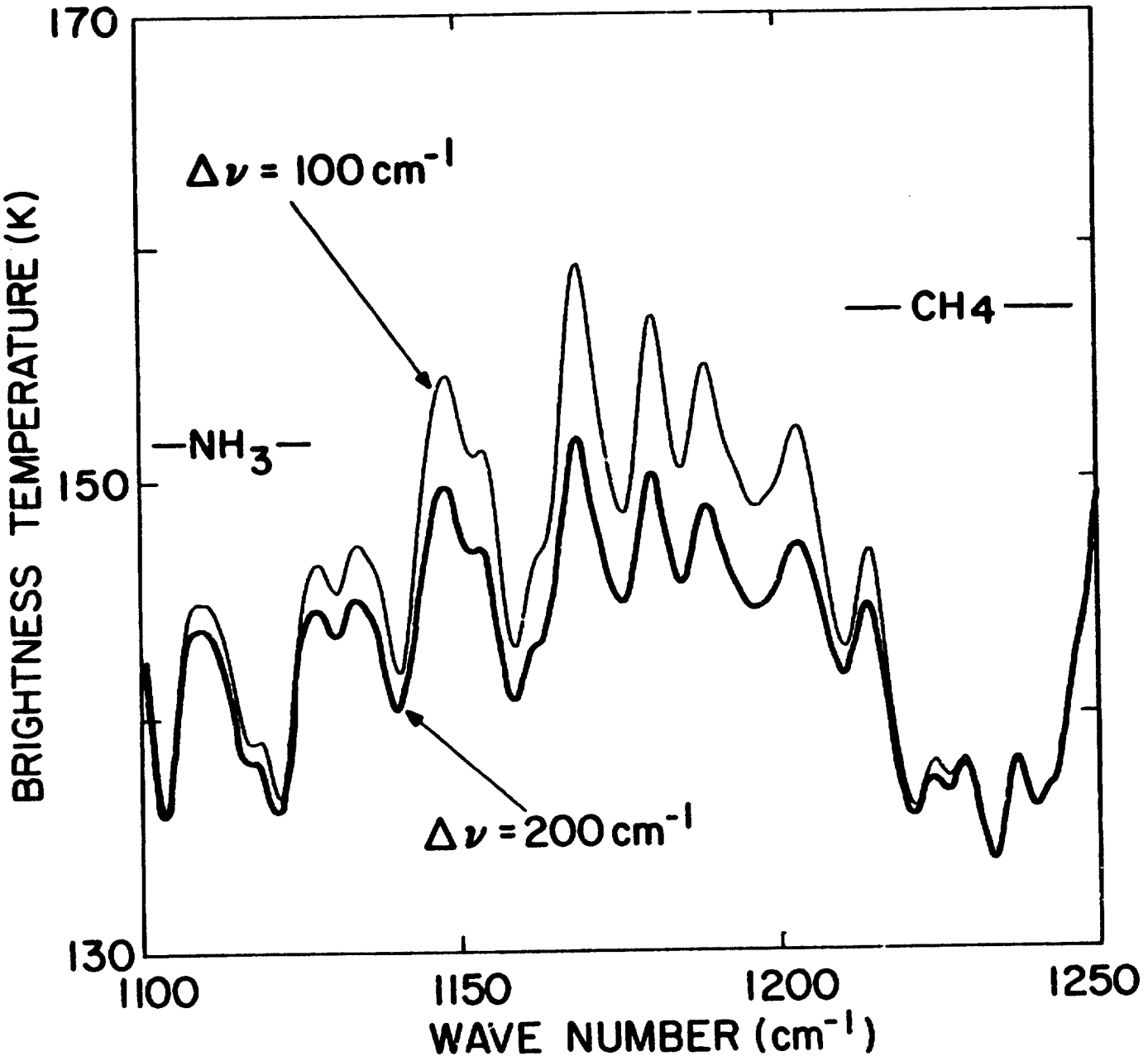
170
150
130
1100
1150
1200
1250
BRIGHTNESS TEMPERATURE (K)
WAVE NUMBER (cm⁻¹)
Δν = 100 cm⁻¹
Δν = 200 cm⁻¹
—NH3—
— CH4 —

FIGURE 9

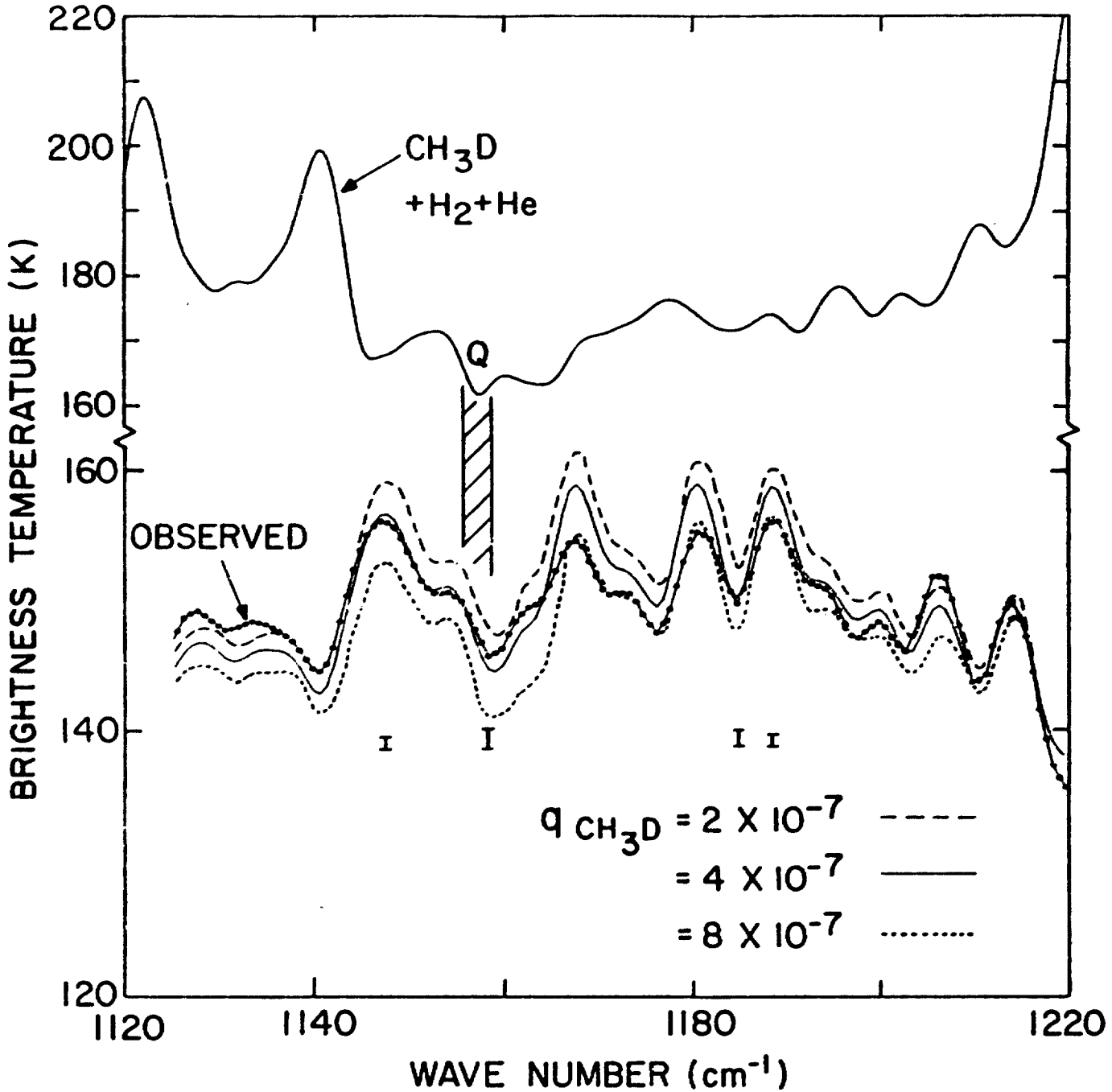
220
200
180
160
160
140
120
BRIGHTNESS TEMPERATURE (K)
CH_3D
$+H_2+He$
Q
OBSERVED
I
I
I I
$q_{CH_3D} = 2 \times 10^{-7}$
$= 4 \times 10^{-7}$
$= 8 \times 10^{-7}$
1120
1140
1180
1220
WAVE NUMBER (cm^{-1})

FIGURE 10

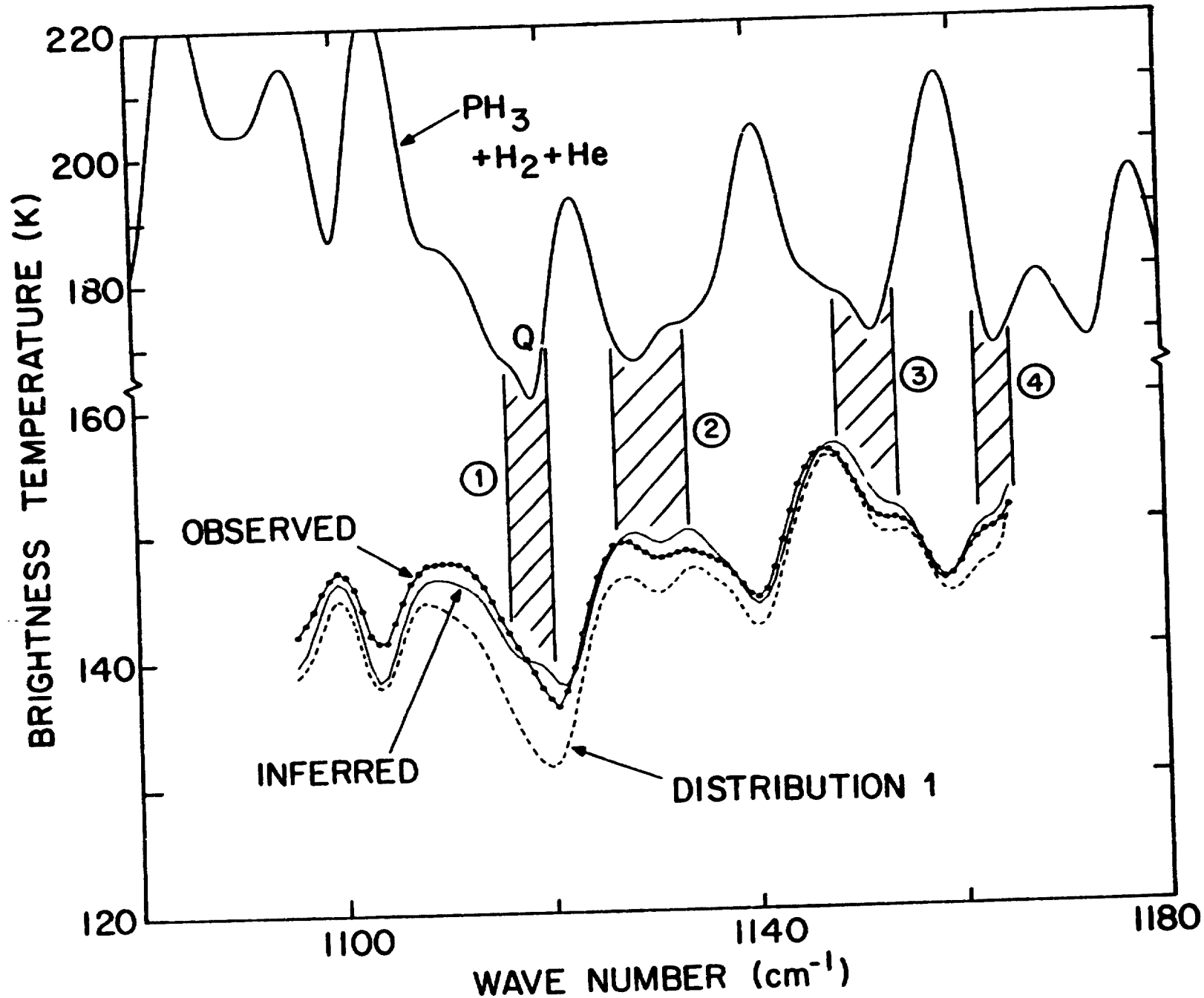
220
200
180
160
140
120
BRIGHTNESS TEMPERATURE (K)
PH3
+H2+He
Q
1
2
3
4
OBSERVED
INFERRED
DISTRIBUTION 1
1100
1140
1180
WAVE NUMBER (cm-1)

FIGURE 11

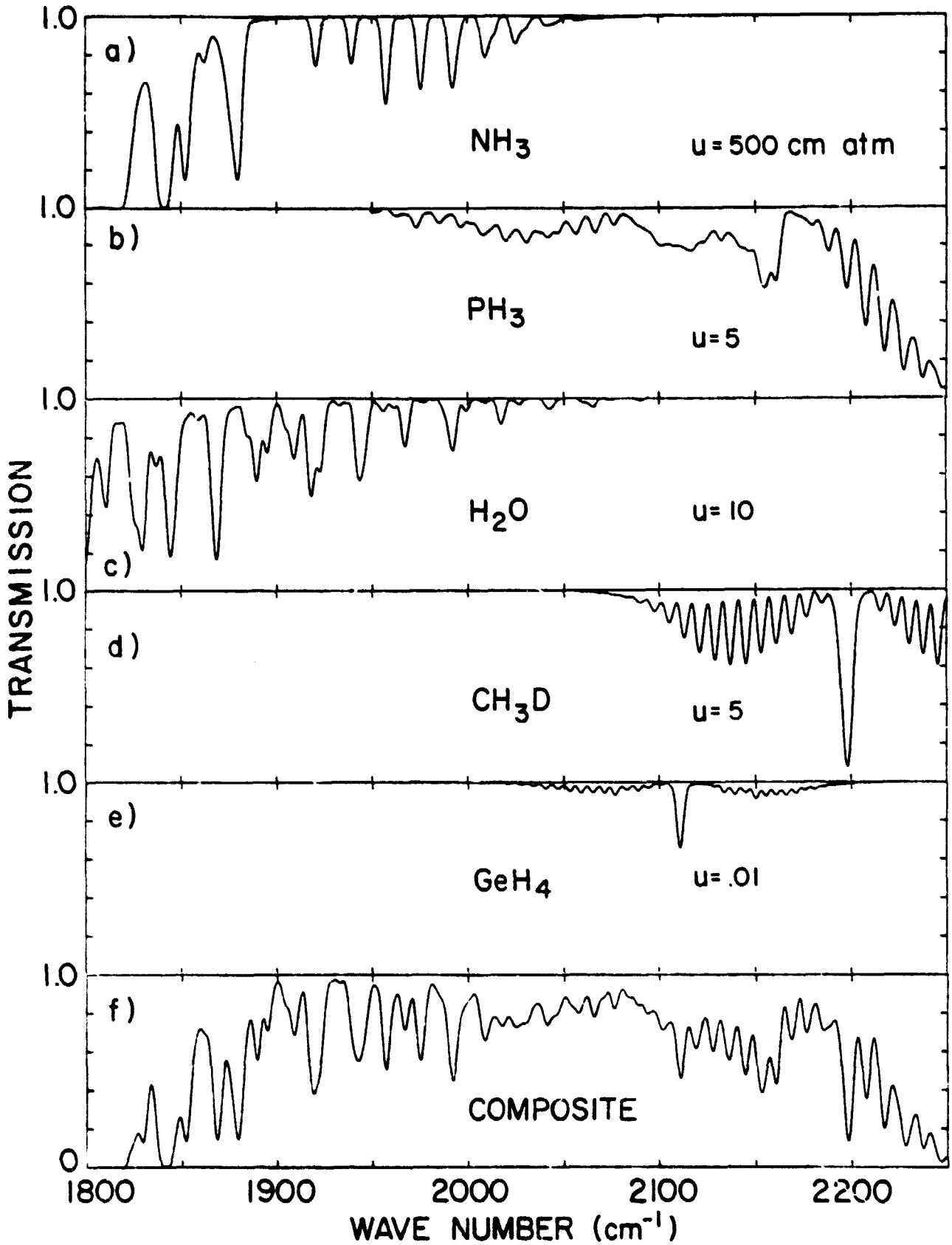
1.0
a)
NH3
u = 500 cm atm
1.0
b)
PH3
u = 5
1.0
c)
H2O
u = 10
1.0
d)
CH3D
u = 5
1.0
e)
GeH4
u = .01
1.0
f)
COMPOSITE
0
TRANSMISSION
1800
1900
2000
2100
2200
WAVE NUMBER (cm-1)

FIGURE 12

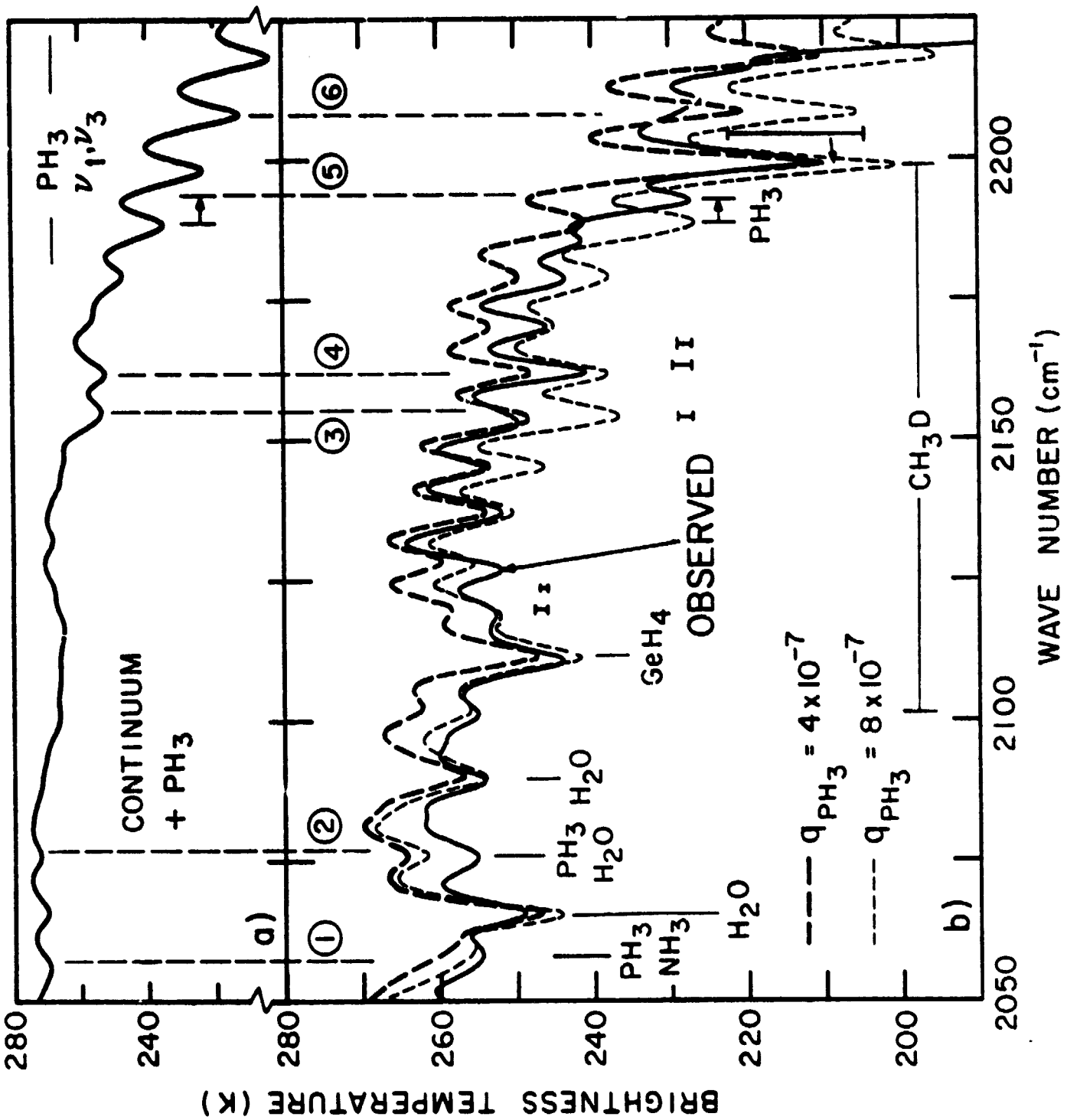
BRIGHTNESS TEMPERATURE (K)
280
240
280
260
240
220
200
2050
2100
2150
2200
WAVE NUMBER (cm⁻¹)
a)
b)
CONTINUUM
+ PH3
PH3
ν1,ν3
OBSERVED I II
I1
I2
GeH4
PH3 H2O
H2O
PH3
NH3
H2O
PH3
CH3D
qPH3 = 4x10⁻⁷
qPH3 = 8x10⁻⁷
①
②
③
④
⑤
⑥

FIGURE 13

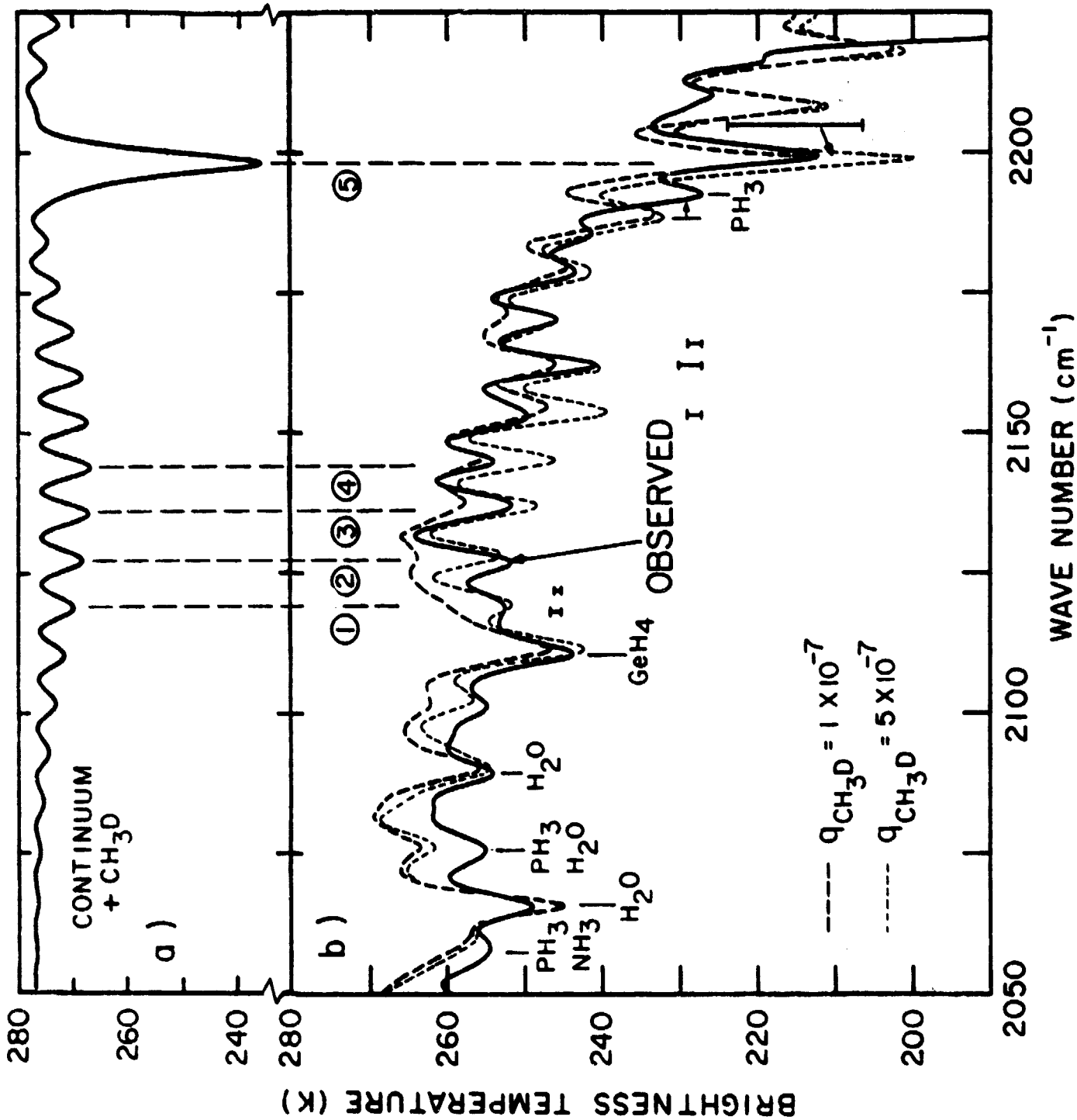
CONTINUUM
+ CH_3D
a)
b)
OBSERVED
PH_3
NH_3
H_2O
GeH_4
$q_{CH_3D} = 1 \times 10^{-7}$
$q_{CH_3D} = 5 \times 10^{-7}$
BRIGHTNESS TEMPERATURE (K)
WAVE NUMBER (cm^{-1})

FIGURE 14

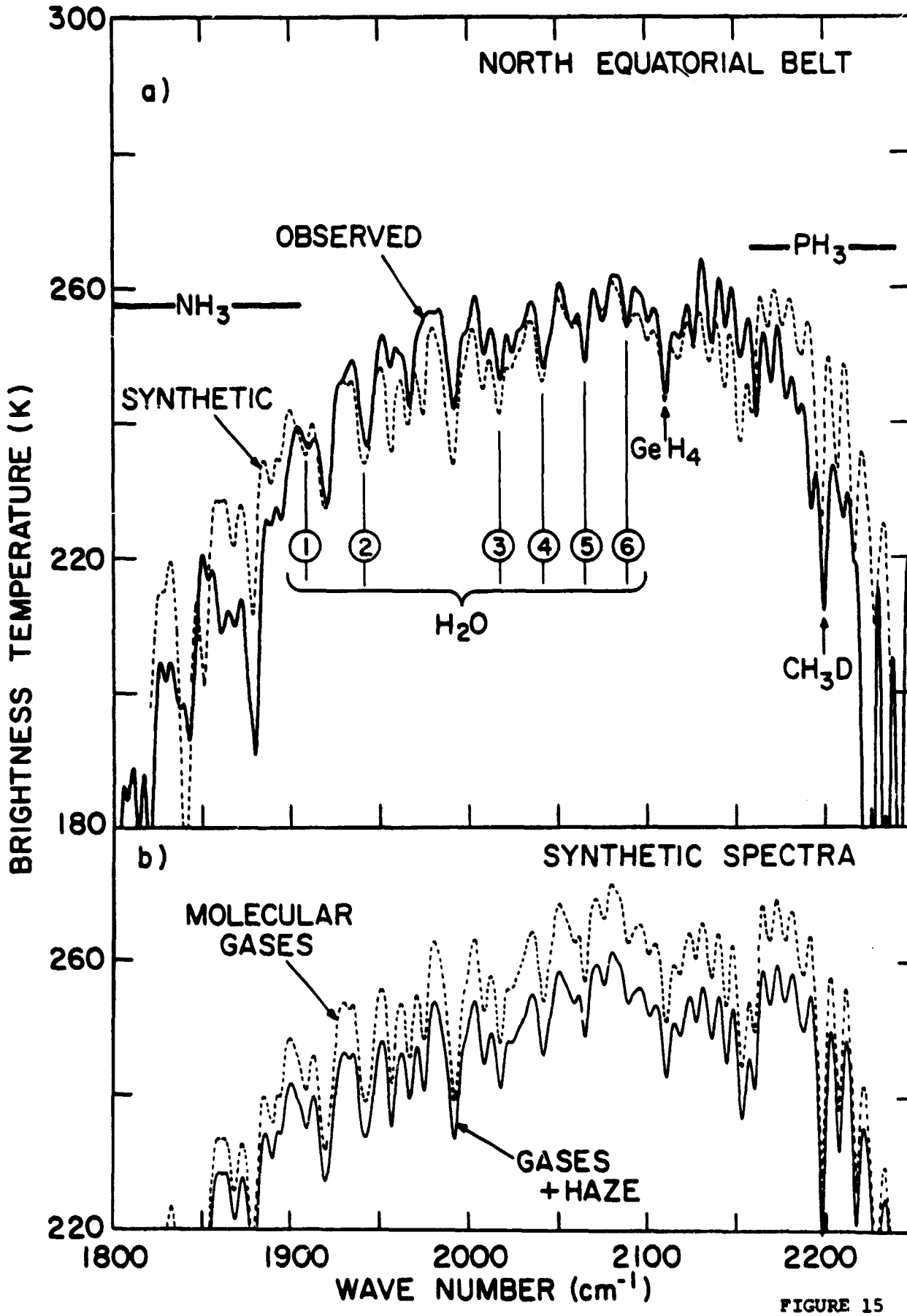
300
260
220
180
NORTH EQUATORIAL BELT
a)
OBSERVED
SYNTHETIC
NH3
PH3
GeH4
CH3D
H2O
1
2
3
4
5
6
BRIGHTNESS TEMPERATURE (K)
b)
SYNTHETIC SPECTRA
MOLECULAR GASES
GASES +HAZE
260
220
1800
1900
2000
2100
2200
WAVE NUMBER (cm-1)

FIGURE 15

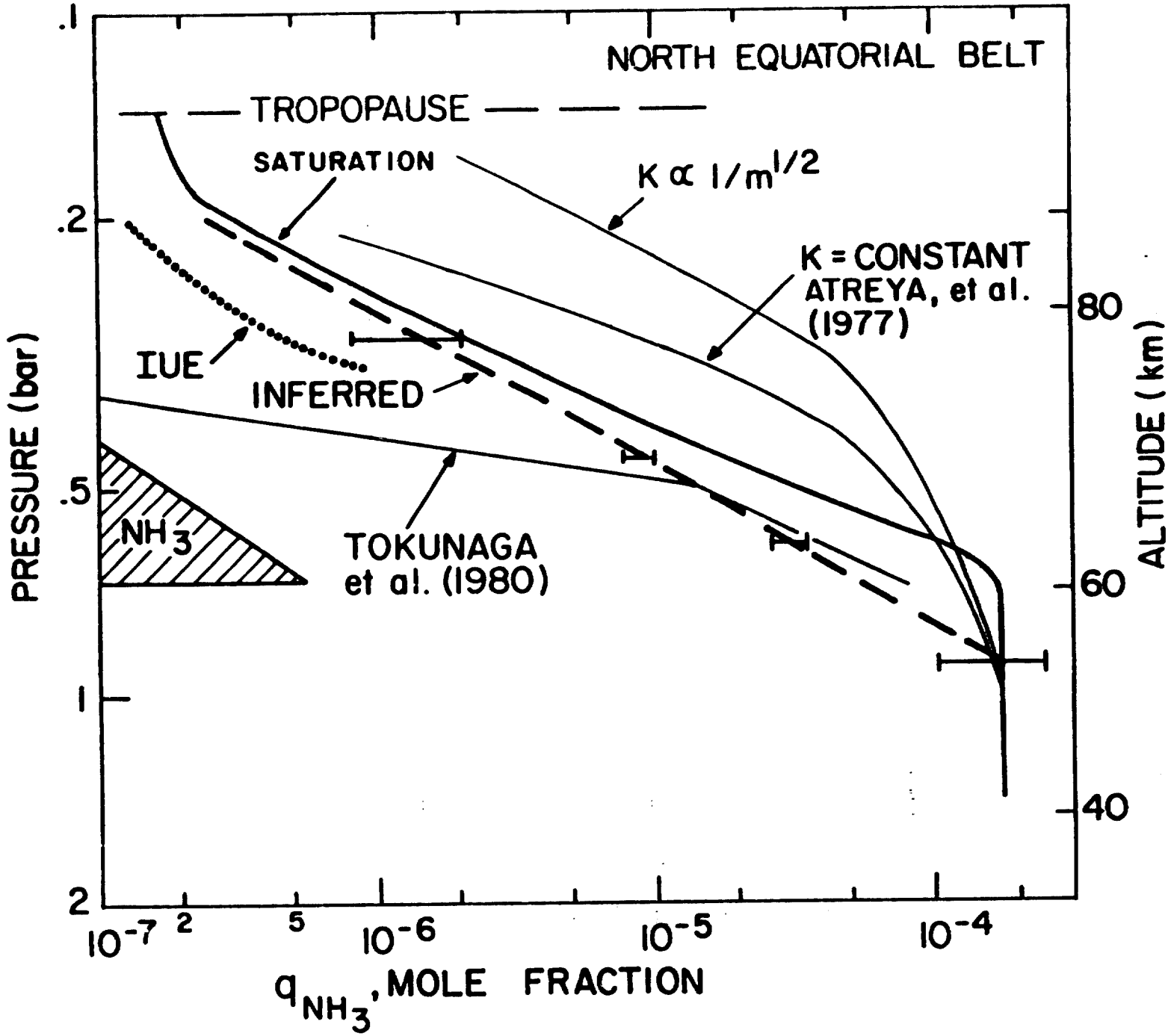
NORTH EQUATORIAL BELT
TROPOPAUSE
SATURATION
K α 1/m^1/2
K = CONSTANT
ATREYA, et al.
(1977)
IUE
INFERRED
NH3
TOKUNAGA
et al. (1980)
PRESSURE (bar)
ALTITUDE (km)
.1
.2
.5
1
2
80
60
40
10^-7
2
5
10^-6
10^-5
10^-4
q_NH3, MOLE FRACTION

FIGURE 16

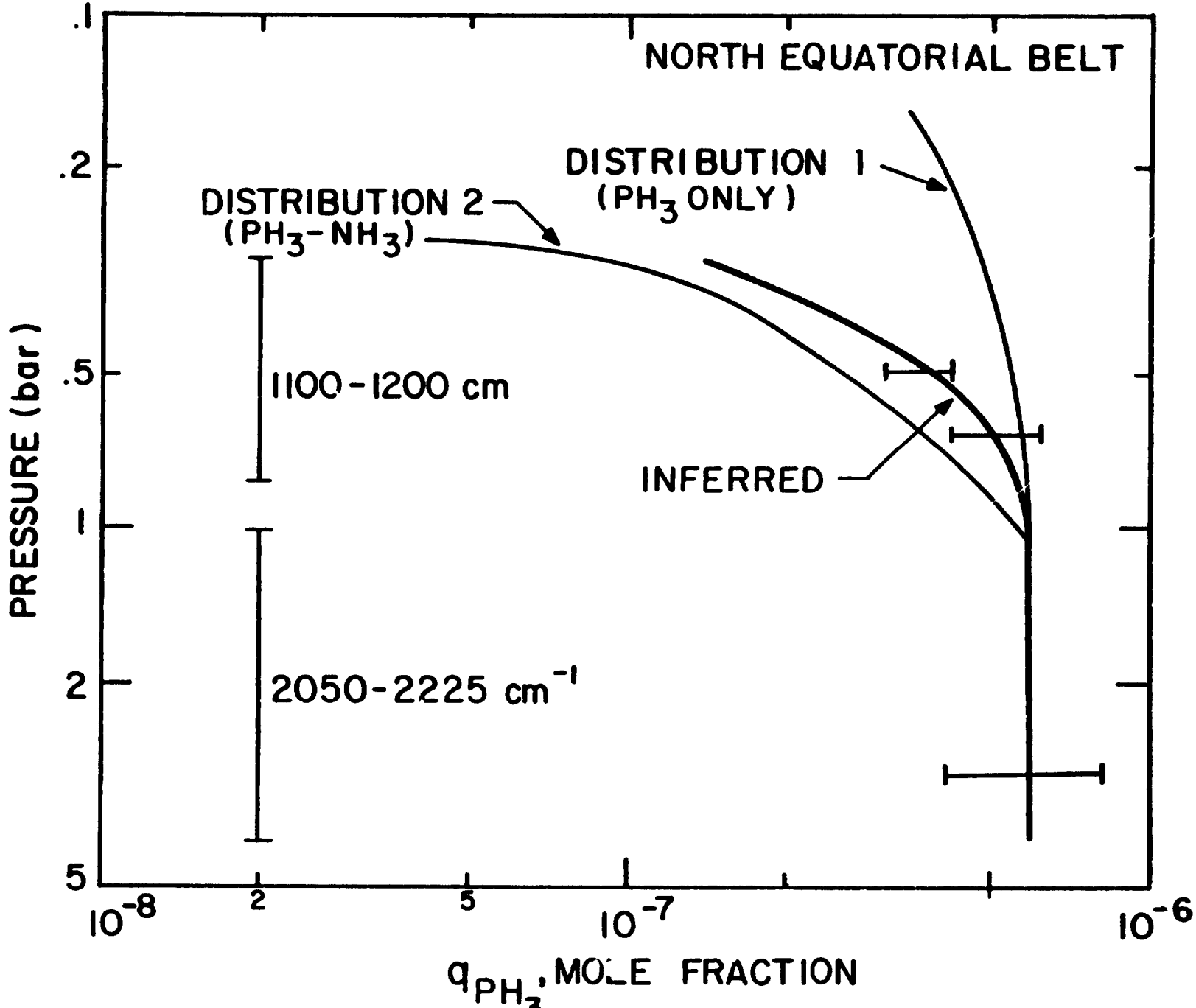
NORTH EQUATORIAL BELT
DISTRIBUTION 1
(PH3 ONLY)
DISTRIBUTION 2
(PH3-NH3)
1100-1200 cm
INFERRED
2050-2225 cm-1
PRESSURE (bar)
.1
.2
.5
1
2
5
10-8
2
5
10-7
10-6
qPH3, MOLE FRACTION

FIGURE 17

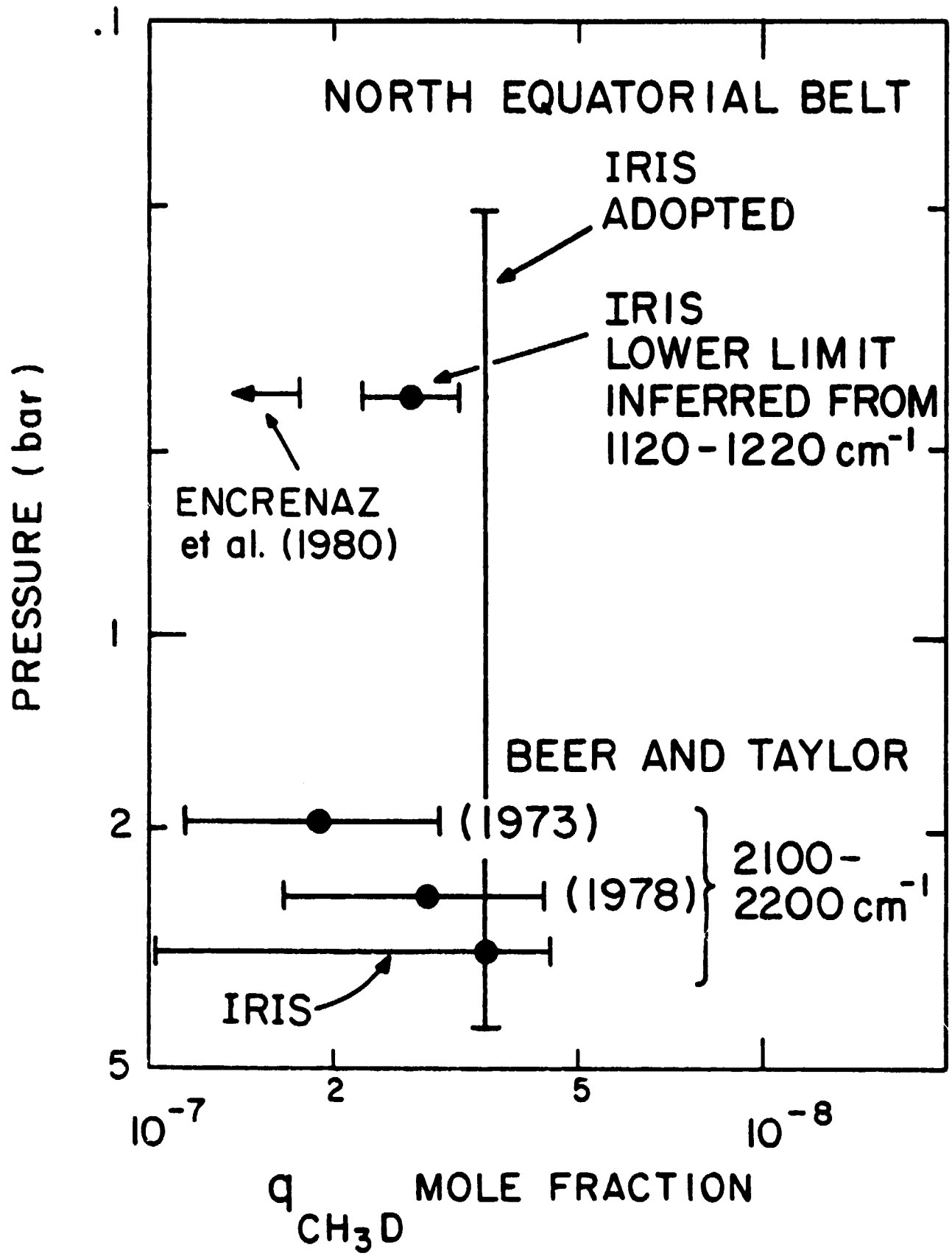
.1
NORTH EQUATORIAL BELT
IRIS
ADOPTED
IRIS
LOWER LIMIT
INFERRED FROM
1120-1220 cm⁻¹
ENCRENAZ
et al. (1980)
PRESSURE (bar)
1
BEER AND TAYLOR
2
(1973)
(1978)
2100-
2200 cm⁻¹
IRIS
5
2
5
10⁻⁷
10⁻⁸
q CH3D MOLE FRACTION

FIGURE 18

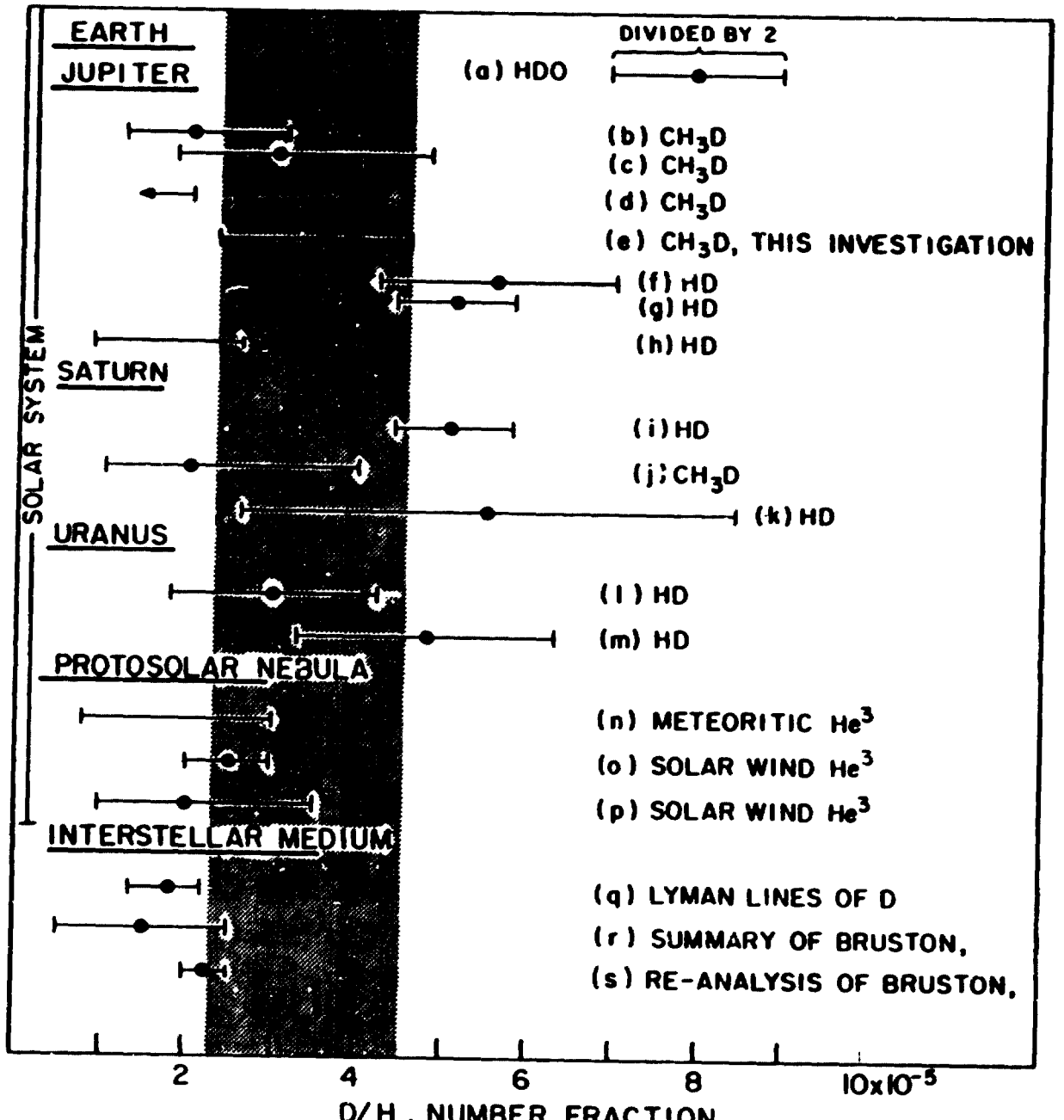
EARTH
JUPITER
SATURN
URANUS
PROTOSOLAR NEBULA
INTERSTELLAR MEDIUM
SOLAR SYSTEM
DIVIDED BY 2
(a) HDO
(b) CH_3D
(c) CH_3D
(d) CH_3D
(e) CH_3D, THIS INVESTIGATION
(f) HD
(g) HD
(h) HD
(i) HD
(j) CH_3D
(k) HD
(l) HD
(m) HD
(n) METEORITIC He^3
(o) SOLAR WIND He^3
(p) SOLAR WIND He^3
(q) LYMAN LINES OF D
(r) SUMMARY OF BRUSTON,
(s) RE-ANALYSIS OF BRUSTON,
2
4
6
8
10×10^{-5}
D/H, NUMBER FRACTION

FIGURE 19

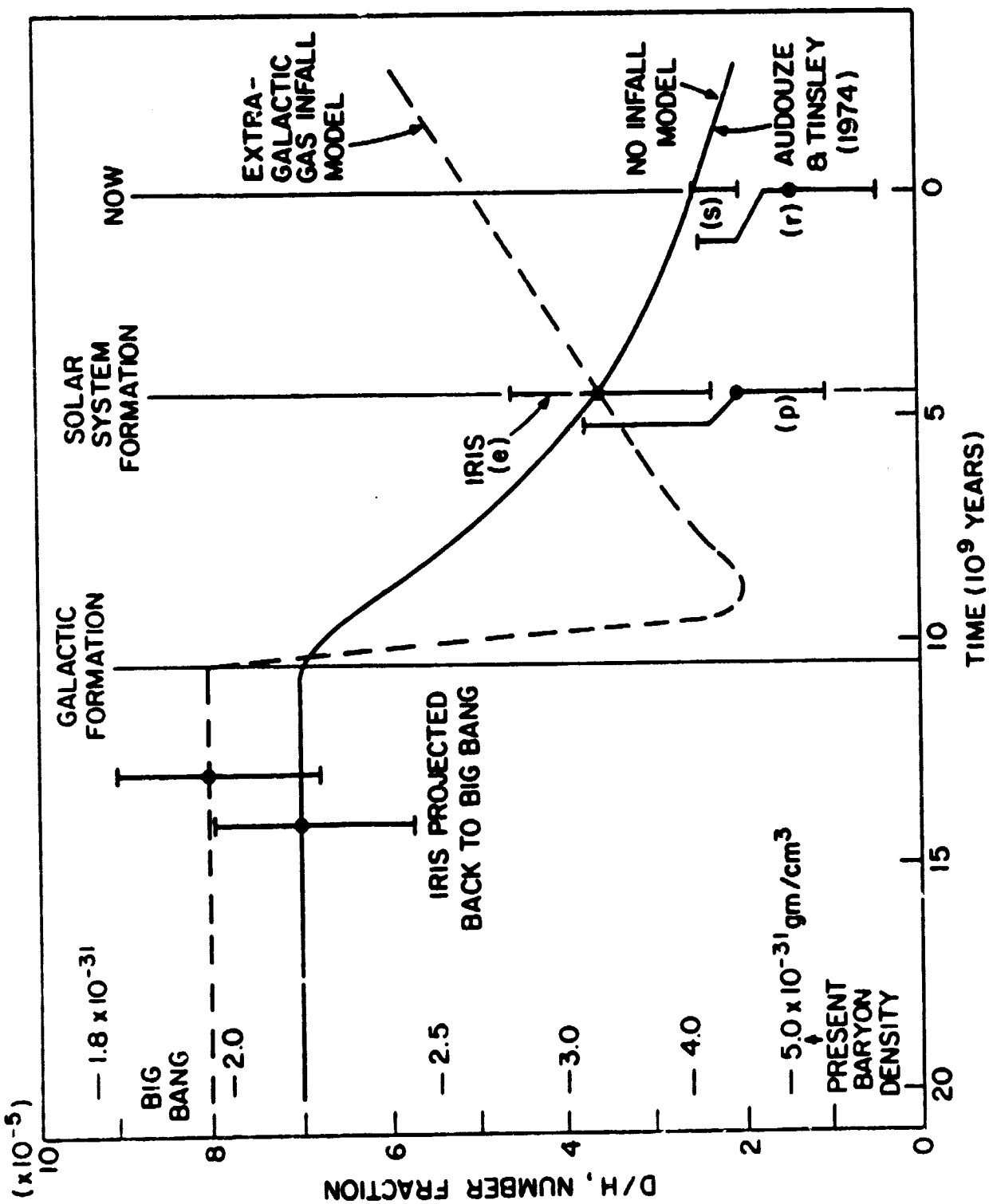
(x10⁻⁵)
D/H, NUMBER FRACTION
TIME (10⁹ YEARS)
NOW
SOLAR SYSTEM FORMATION
GALACTIC FORMATION
BIG BANG
EXTRA-GALACTIC GAS INFALL MODEL
NO INFALL MODEL
AUDOUZE & TINSLEY (1974)
IRIS (e)
(p)
(s)
(r)
IRIS PROJECTED BACK TO BIG BANG
PRESENT BARYON DENSITY
1.8 x 10⁻³¹
2.0
2.5
3.0
4.0
5.0 x 10⁻³¹ gm/cm³

FIGURE 20